EXPERIMENTAL INVESTIGATION OF AGITATION HYDRODYNAMICS AND MIXING-TIME OF NON-NEWTONIAN SOLUTIONS

A THESIS SUBMITTED TO
THE GRADUATE SCHOOL OF NATURAL AND APPLIED SCIENCES
OF
MIDDLE EAST TECHNICAL UNIVERSITY

BY

BEGÜM ŞEN

IN PARTIAL FULFILLMENT OF THE REQUIREMENTS
FOR
THE DEGREE OF MASTER OF SCIENCE
IN
CHEMICAL ENGINEERING

DECEMBER 2011

Approval of the thesis:

EXPERIMENTAL INVESTIGATION OF AGITATION HYDRODYNAMICS AND MIXING-TIME OF NON-NEWTONIAN SOLUTIONS

submitted by **BEGÜM ŞEN** in partial fulfillment of the requirements for the degree of **Master of Science in Chemical Engineering Department, Middle East Technical University** by,

Prof. Dr. Canan Özgen _____
Dean, Gradute School of **Natural and Applied Sciences**

Prof. Dr. Deniz Üner _____
Head of Department, **Chemical Engineering Dept.**

Assoc. Prof. Dr. Yusuf Uludağ _____
Supervisor, **Chemical Engineering Department**

Examining Committee Members:

Prof. Dr. Göknur Bayram _____
Chemical Engineering, METU

Assoc. Prof. Dr. Yusuf Uludağ _____
Chemical Engineering, METU

Assoc. Prof. Dr. Halil Kalıpçılar _____
Chemical Engineering, METU

Assist. Prof. Dr. Serkan Kıncal _____
Chemical Engineering, METU

Prof. Dr. Serkan Özgen _____
Aerospace Engineering, METU

Date: _____

I hereby declare that all information in this document has been obtained and presented in accordance with academic rules and ethical conduct. I also declare that, as required by these rules and conduct, I have fully cited and referenced all material and results that are not original to this work.

Name, Last Name: Begüm Şen

Signature :

ABSTRACT

EXPERIMENTAL INVESTIGATION OF AGITATION HYDRODYNAMICS AND MIXING-TIME OF NON-NEWTONIAN SOLUTIONS

Şen, Begüm

M.Sc. Department of Chemical Engineering

Supervisor: Assoc. Prof. Dr. Yusuf Uludağ

December 2011, 75 pages

Mixing is a crucial process for many large scale and small scale applications from food industry to cosmetics, from drug industry to petrochemical processes, etc. Changes in parameters (temperature, viscosity, velocity distribution, etc.) during the mixing affect the production process and the end product quality and the cost. Thus, these parameters, mostly the hydrodynamic parameters, should be monitored closely during the process. In order to ensure good and efficient mixing in the solution, high degree of turbulence is maintained while dead zones in the tank should be avoided.

In chemical industry, the mixing processes generally involve complex solutions that exhibit non-Newtonian flow behavior that merits a study on the agitation hydrodynamics and mixing time. Thus, in this study agitation of carboxymethyl cellulose (CMC) solution in a laboratory scale mixing tank is investigated. The effects of CMC concentration and agitation speed on the hydrodynamics of the solution and mixing time are studied in detail. CMC concentrations studied are 0.5

wt%, 1 wt% and 2 wt%. Impeller speeds, on the other hand, are set as 150 rpm, 300 rpm and 600 rpm.

The hydrodynamics of mixing can be studied easily by Ultrasound Doppler Velocimetry (UDV) which is a fast, non-invasive measuring technique in fluid dynamics. Also, the mixing time measurements were carried out through electrical conductivity of the agitated solution.

UDV results show that the flow field has a typical pattern produced by the Rushton turbine. The main characteristics of the flow are that, in the impeller region radial components of the flow dominate. Near the wall flow occurs mainly in the axial direction towards the top and bottom of the tank.

Mixing time measurements reveal that mixing time increases with decreasing impeller speed and with increasing solution concentration (i.e. viscosity). Typical mixing time values are in the range of 250-2600 seconds for different impeller speeds and CMC concentrations.

KEYWORDS: Agitation Hydrodynamics, Ultrasound Doppler Velocimeter, Mixing Time, Non-Newtonian Fluids

ÖZ

NEWTONUMSU OLMAYAN AKIŞKANLARIN KARIŞTIRMA HİDRODİNAMİĞİNİN VE KARIŞIM ZAMANININ DENEYSEL OLARAK İNCELENMESİ

Şen, Begüm

Yüksek Lisans, Kimya Mühendisliği Bölümü

Tez Yöneticisi: Assoc. Dr. Yusuf Uludağ

Aralık 2011, 75 sayfa

Karıştırma hem büyük hem küçük ölçekli süreçlerin önemli bir parçasıdır ve gıdadan kozmetiğe, ilaçtan petrokimyaya, v.b. birçok üretim sürecinde kullanılmaktadır. Karıştırma sırasındaki parametrelerdeki değişiklikler (sıcaklık, viskozite, hız dağılımı, v.b.) üretim sürecini ve son ürünün kalite ve fiyatını etkilemektedir. Bu yüzden, bu parametreler, özellikle hidrodinamiğe bağlı olanlar, süreç boyunca yakından takip edilmelidir. İyi ve etkili bir karıştırmayı sağlamak için, tanktaki "ölü noktalardan" kaçınmak için ileri derecede türbülans tercih edilir.

Kimya sanayinde, karıştırma prosesleri genelde Newtonumsu olmayan kompleks çözeltileri içermektedir ki bu çözeltilerin karıştırma hidrodinamiği ve zamanı üzerine çalışmalar yapılmalıdır. Bu nedenle, bu çalışmada, karboksimetil selüloz (CMC) çözeltilerinin karıştırılması laboratuvar ölçekli bir karıştırma tankında incelenmiştir. CMC derişiminin ve karıştırma hızının, çözeltinin hidrodinamiği ve karıştıma zamanı üzerindeki etkileri detaylı olarak çalışılmıştır. Çalışmada kütlece

yüzde 0.5, 1 ve 2'lik çözeltiler kullanılmıştır. Pervane hızları 150 rpm, 300 rpm ve 600 rpm arasında değiştirilmiştir.

Karıştırma olayının hidrodinamiği akışkanlar dinamiğinde hızlı ve tahribatsız bir ölçüm tekniği olarak kullanılan Ultrasonik Dopler Hız Ölçüm (UDV) cihazı ile elde edilmiştir. Ayrıca, karıştırmanın tamamlanma süresi de çözeltinin iletkenlik ve derişimine bağlı bir korelasyon kullanılarak incelenmiştir.

UDV sonuçları, akışın Rushton türbini ile oluşturulmuş tipik bir modele sahip olduğunu göstermektedir. Akışın ana özelliklerine göre, pervane yakınında radiyal bileşenler daha güçlüdür. Tank duvarları yakınındaki akış, temel olarak eksenel yönde tank tabanı ve üst bölümlerine doğrudur.

Karıştırma zamanı ölçümleri, karıştırmanın tamamlanma süresi azalan pervane hızı ve artan çözelti derişimi (bir anlamda viskozite) ile arttığını göstermektedir. Farklı pervane hızları ve CMC derişimleri için tipik karıştırma süreleri 250-2600 saniye aralığındadır.

ANAHTAR KELİMELER: Karıştırma Hidrodinamiği, Ultrasonik Doppler Hız Ölçüm Cihazı, Karıştırma Süresi, Newtonumsu Olmayan Akışkanlar

To Doğanay and GSL,

ACKNOWLEDGEMENTS

I would like to thank to my supervisor Assoc. Prof. Dr. Yusuf Uludağ for his patience, support, encouragements, supervision and suggestions throughout my study.

I would like to thank the Machine Shop technicians of the Chemical Engineering Department for their help during my study.

My sincere thanks are for my eternal roommate Nazlı Fidan for being my tenacious friend during our METU life.

I am very glad to have innumerable friends in chemical engineering who gave me enthusiasm for my thesis study.

I appreciate all kinds of support given by Mehlika Mete who enabled so many things for years.

Finally, I would like to express my profound gratitude to Doğanay Doğan for his affectionate support and faith throughout my life.

TABLE OF CONTENTS

LIST OF TABLES

TABLES

LIST OF FIGURES

FIGURES

LIST OF SYMBOLS

c	Speed of sound (m/s)
C	Concentration of NaCl in polymer solution (M)
C*	Initial concentration of NaCl in polymer solution (M)
D_t	Tank diameter (m)
D_i	Impeller diameter (m)
f_d	Doppler frequency (MHz)
f_e	Ultrasound emission frequency (MHz)
g	Gravity (m/s^2)
h	Impeller bottom clearance (m)
H	Liquid height (m)
m	Consistency factor ($Pa.s^m$)
n	Flow index
N	Impeller speed (s^{-1})
N_p	Power number
p	Depth of particle
P	Power (W)
r	Distance from tank center (m)
R	Radius of tank (m)
Re	Reynolds number
t_m	Mixing time (s)
T_d	Delay time (s)
T	Torque (N.m)
U_{tip}	Impeller tip velocity (mm/s)
V	Velocity (mm/s)
V_r	Radial component of velocity (mm/s)
V_r^*	Dimensionless radial component of the velocity

V_t	Tangential component of velocity (mm/s)
V_t^*	Dimensionless tangential component of the velocity
y	Distance from tank wall (mm)
z	Distance from the tank bottom (mm)
z^*	Dimensionless distance from the tank bottom

Greek Letters

Δ	Difference between the data
γ	Shear rate (s^{-1})
η	Apparent viscosity (Pa.s)
μ	Dynamic viscosity (Pa.s)
ν	Kinematic viscosity
ρ	Density (kg/m^3)
τ	Shear stress (Pa)

Abbreviations

CMC	Carboxymethyl cellulose
PRF	Pulse Repetition Frequency
UDV	Ultrasound Doppler Velocimeter

CHAPTER 1

INTRODUCTION

Mixing is a phenomenon benefited not only for large scale applications (industrial vessels) but also for small scale applications (kitchen pots). It is very crucial in many of the important processes such as cosmetics, pharmaceuticals, food, petrochemicals, etc.

The parameters defined for mixing processes can radically change the production processes and the quality of the final products. Hydrodynamics in the mixing vessel, geometry of the vessel, type and position of the impeller, mixing duration and power consumption of the impeller are the parameters identifying the mixing characteristics and requirements of any mixing system. Keeping track of these parameters during the production processes involving mixing is a critical subject to be investigated deeply.

There are two types of mixing: laminar and turbulent. Although laminar mixing has its difficulties and has been studied in the past **[1]** by many authors, in most industrial applications where large scale stirring vessels are used, turbulence is predominant. Turbulent flows are far more complicated and it is a challenging task to predict due to their chaotic nature.

Up to now, the hydrodynamics of mixing phenomena have been under investigation using different methods. Some of the methods used to determine the velocity profile of a system are Laser Doppler Velocimetry (LDV), Ultrasound Doppler Velocimeter (UDV), Nuclear Magnetic Resonance (NMR) and image processing techniques. To be able to use some of these methods, one has to accomplish many specific

requirements: working with a transparent medium/vessel, disturbing the medium under investigation, adding tracers, long analysis durations, etc. However, working on transparent medium, accompanied with a transparent vessel, is not always possible. Especially, in industry, one has to get the results quickly and should not disturb the system. One of the mentioned methods, Ultrasound Doppler Velocimeter, is very promising in raising the amount of the studies on hydrodynamics because this technique can be applied to both transparent and opaque vessels, it can provide the results quickly and the system can be analyzed without disturbances **[1].**

Furthermore, most of the fluids used in the industry have non-Newtonian characteristics: the world is not ideal, many of the data obtained in this area empirical rather than theoretical. Rheological properties of this kind of fluids sharply affect the hydrodynamics of agitation. However, the studies on the agitation of non-Newtonian fluids are not enough yet because there are lots of parameters to be investigated deeply.

Since reaching turbulent conditions especially for high-viscosity solutions is not an easy task, it is difficult to increase mixing efficiency. Thus, scientists are trying different kinds of impeller to increase the efficiency **[2]**. Also, to follow the mixing completion time is necessary for time and energy efficiency of the processes. For mixing time of non-Newtonian solutions, more studies are required **[3]**, **[4]**.

Due to reasons explained above, the objective of this study is to investigate the agitation hydrodynamics and the mixing time of a shear-thinning non-Newtonian solution, in an agitated tank via Ultrasound Doppler Velocimeter and a technique based on the conductance of solution.

CHAPTER 2

LITERATURE SURVEY

Velocity profile distribution gives the opportunity to identify characteristics of any flow. The scientists for many years tried to find better methods to visualize the flow. There are several studies investigating the velocity field in agitated tanks. In **Figure 2.1,** an example of velocity vector field obtained using a computational method is given **[5].**

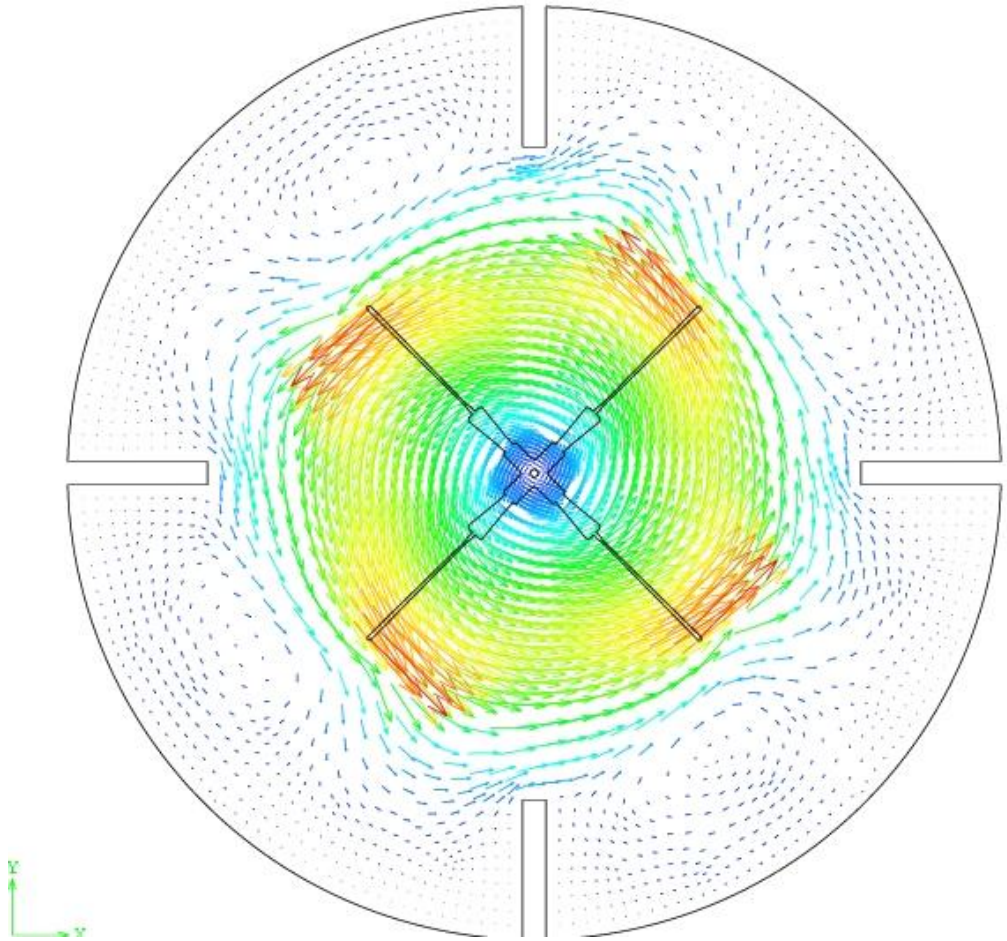

Figure 2.1 Mean Velocity Vector Plot in Disc Center-plane **[5]**

Turbulence is important for efficient mixing, especially to prevent the formation of the dead-zones. Jaafar et al. have investigated the velocity and turbulence characteristics of a pipe system containing water with impurities via Ultrasound Pulse Doppler Velocimetry. The result was that there is a good agreement between experimental velocity profiles and theoretical models **[6].**

Hui has studied hydrodynamics of pulp suspensions in a cylindrical vessel with axial flow impellers. He demonstrated that UDV is applicable to opaque pulp suspensions **[7].**

Pfund and his coworkers have focused on the capabilities of UDV in a pipe flow of carbopol. This study shows that UDV is a non-invasive technique and it does not interrupt the process. Also, it can supply continuous output **[8].**

Doğan has investigated polydimethylsiloxane melt in a pipe system via UDV. This study showed that when velocity resolution better, the minimum shear rate to be accurately measured is lower **[9].**

Uludağ and his coworkers worked on a pipe system containing xanthan gum via UDV. According to the results of this study, better results can be obtained at higher flow rates. Using UDV, viscosity can be obtained in a wide range of shear rates in a few minutes **[1].**

The investigation of opaque liquids is still under development. In 1987, Takeda has showed that UDV is useful for low temperature melts of metals **[10].** However, it should be noted that even UDV does not provide very reliable results for high temperature melts of metals **[11].**

Laser Doppler Velocimetry (LDV) is a technique based on the optical determination of the velocity. LDV is also called Laser Doppler Anemometry (LDA). LDV is developed by Yeh et al. **[12]** in 1964 and it has been used in several studies to study the hydrodynamics. In this technique, the Doppler shift of the laser radiations, which are scattered by the moving particles, is measured and processed via signal processing equipments in order to calculate the velocity of the particles. LDV does not disturb the process under investigation. It is applicable to either gas or liquid

media. However, it requires transparent media due to optical concerns which is an important drawback compared to UDV.

Operation parameters of industrial scale processes are sometimes too complex to be obtained in laboratory scale experiments. Also, sometimes simulating the experiment in laboratory is too expensive. Computational techniques can significantly reduce the cost of simulating the experiments to investigate the necessary characteristics. However, to accept the computational results as reliable enough to influence design decisions, the computational model must be validated through experimental data **[13].**

In 2009, Broniarz and his coworkers have studied mixing time of polymer solutions such as CMC, guar gum and polyacrylamide via conductometric methods. They have concluded that there are differences in interactions of anionic and non-ionic polymers for mixing time due to macromolecular configurations in the solution **[14].**

Khopkar et al. has worked on CMC and glucose solutions using discoloration method. This study showed that for shear thinning fluids, the mixer has difficulties in achieving complete homogeneity around the central shaft **[2].**

Another study on the mixing time of polymer solutions is carried by Montante et al. They have compared CFD results with conductometric measurements for water, polyvinylpyrolidine and carbomer solutions. Their studied proposed that exact location of probes and tracer injection is not significant **[3].**

In industrial mixing applications, the power consumption per unit volume of fluid is used extensively for scaling and design. In spite of its widespread use, the dependence of power consumption on impeller and tank geometry is designed only in general terms. This situation stems from both the difficulty of obtaining accurate torque measurements on small scale and partly from the predictive limitations of drag theory **[15].**

A non-Newtonian fluid is a fluid whose flow properties differ dramatically from those of Newtonian fluids. Generally, the viscosity of non-Newtonian fluids is not independent of shear rate or shear rate history.

Many salt solutions and molten polymers are non-Newtonian fluids such as ketchup, custard, toothpaste, starch suspensions, paint, blood, and shampoo. In a Newtonian fluid, the relation between the shear stress and the shear rate is linear, and the constant of proportionality being the coefficient of viscosity. In a non-Newtonian fluid, the relation between the shear stress and the shear rate is different, and can even be time-dependent. Therefore, a constant coefficient of viscosity cannot be defined.

Carboxymethyl cellulose (CMC) is widely used in the scientific studies since it forms has harmless and cheap non-Newtonian solutions with water. Broniarz et al. studied the heat transfer characteristics in non-Newtonian media using CMC solutions **[16].** They determined the friction factor in boundary layer and the distribution of heat transfer coefficient in CMC solutions.

Dapia et al. has focused on the rheological behavior and solubility of CMC solutions. They concluded that molar mass is related to total degree of substitution **[17].**

CMC solutions have very high viscosities even at small percentages. **Figure 2.2** is taken from the study of Yang et al. **[18]**. This study investigates deeply the properties of CMC solutions. Temperature and concentration dependence of viscosity of CMC solutions is clearly proved in this study. Also, this figure shows high viscosity of even small percentage CMC solutions and shear-thinning behavior.

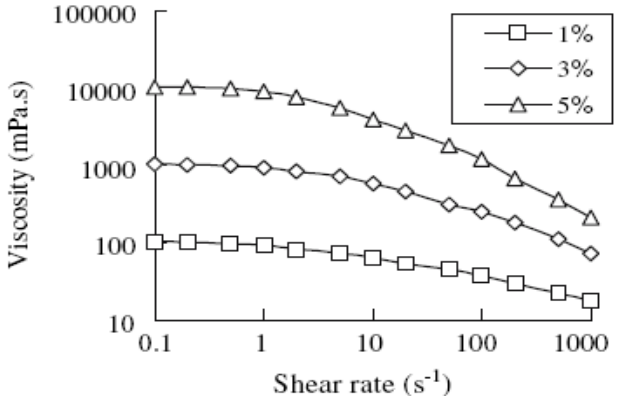

Figure 2.2 Dependence of viscosity of CMC solution upon shear rate at 1, 3, 5 % concentration and 20°C **[18]**

CHAPTER 3

MIXING IN AGITATED TANKS

Agitation is defined in the dictionaries as the act of moving, shaking or disturbing something vigorously. In the case of fluid agitation, Mansour Jahangiri defines it as "introduction of mechanical energy into the vessel by means of a rotating impeller and converting this energy into hydrodynamic motion" **[19].**

Mixing may be required due to several reasons. It can be classified in five agitation operations **[20]:**

- homogenization, i.e. equalization of concentration and temperature differences within the system;
- intensification of heat transfer between a liquid and a heat transfer surface;
- suspension (and possible dissolution) of a solid in a liquid or slurry formation;
- dispersion (or emulsification) of two immiscible liquids in each other;
- dispersion (or sparging) of a gas in a liquid (gas-liquid contacting).

Mixing may seem to be a macro-scale operation. However, there are micro-scale events during the mixing operation. These events are:

- Convection: Fluid moves through the different parts of vessel, preventing stratification.
- Macro-mixing: Separates bulk of fluid into smaller elements.
- Laminar shear: Below the scale of macro mixing fluid elements are further dispersed by laminar shearing.

- Micro-mixing: Diffusion of reactants takes place and it is driven only by concentration gradient.

The dimensions of the agitation tank and the dimensions and arrangement of impellers, baffles and other internals influences mixing extent, mixing quality and the amount of energy required for achieving a required degree of agitation. The internal arrangements depend on the objectives of the operation.

Agitation Impellers

Axial flow impellers are efficient for liquid blending and solids suspension, while radial flow impellers are best used for gas dispersion.

Radial flow impellers include flat blade impeller, disk turbine (Rushton) and hollow blade turbine. They produce two circulating loops, one below and one above the impeller. Mixing occurs not only between these two loops but also more slowly within each loop.

Compared to axial flow impellers, radial flow impellers provide higher shear and higher turbulence levels using lower pumping capacity. Radial flow impellers discharge fluid radially outward to the vessel wall (**Figure 3.1**).

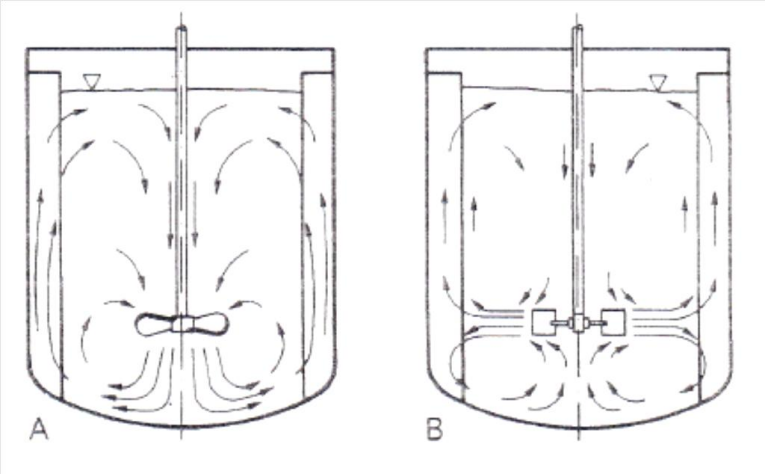

Figure 3.1 Flow patterns in a baffled tank, generated by A) axial-flow propeller and B) radial-flow turbine stirrer **[20]**

Figure 3.2 shows types of impellers according to the predominant flow pattern that they produce, and to the range of viscosities over which they can be effectively used **[20].**

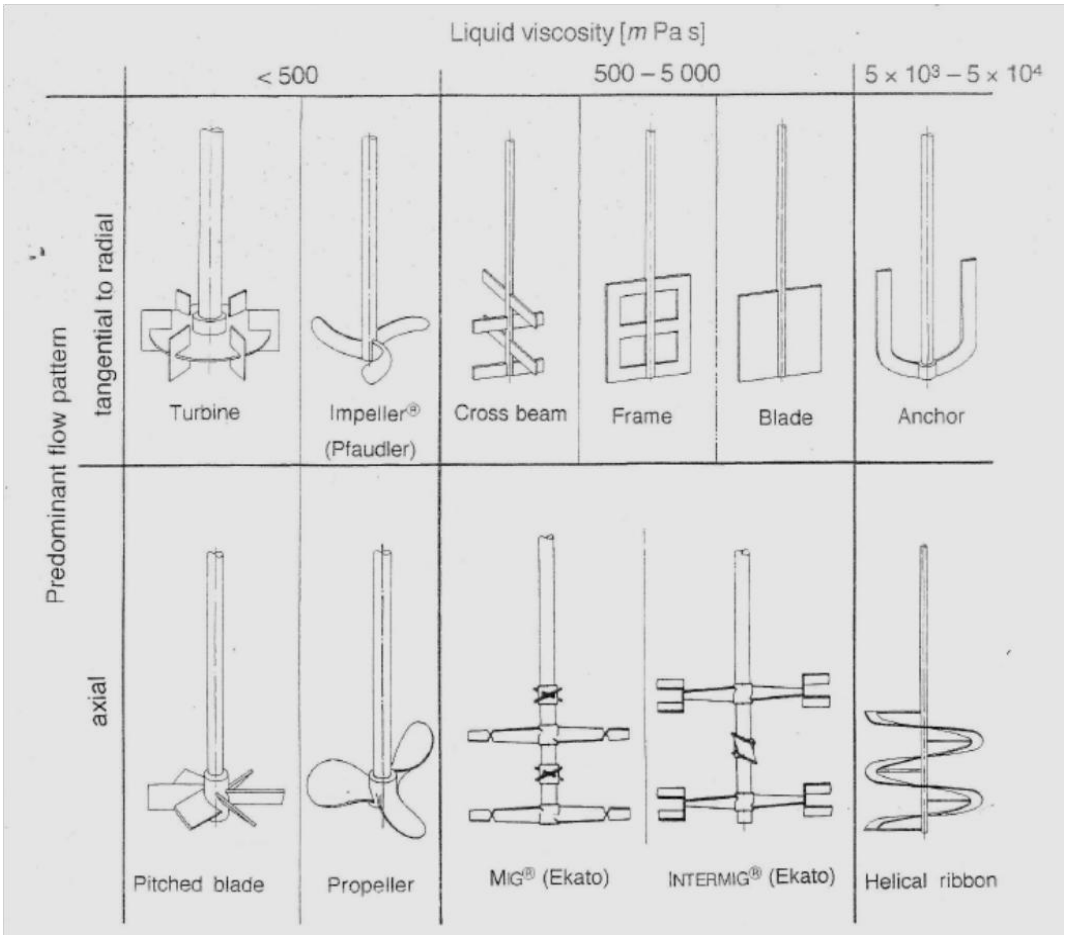

Figure 3.2 Classification of Impellers **[20]**

Impeller size depends on the impeller type and the operating conditions defined by Reynolds, Froude and Power number. For example, the ratio of impeller and tank diameters should be between 0.3-0.6. Lower diameter ratios are preferred for higher impeller speeds.

Rushton turbine is one of the mostly used impeller type to form radial flow. Generally, it consists of a disk and 4 to 6 blades connected perpendicularly to this

disk. The disk part of the Rushton turbine does not affect agitation: it is the blades that support the agitation for this impeller.

Agitation Vessel Geometry

A conventional agitation tank consists of a vessel equipped with a stirrer. The vessel is generally a vertical cylindrical tank. The stirrer has several parts: an impeller, a shaft, a gearbox and a motor drive (**Figure 3.3**).

The shape of agitation tanks can be designed as cylindrical or rectangular. They may have round or flat bottom considering the application area. Although round bottom tanks may require less power than flat bottom tanks.

When a single impeller will be used in an agitation tank, the optimum tank diameter is equal to liquid level with the impeller located at the center for the system.

Except some special cases, which may require pilot plant testing, some general rules have been developed with which mixing equipment can be designed efficiently up to some degree.

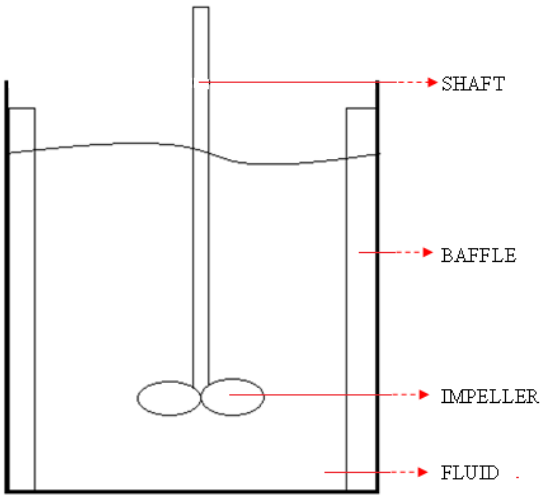

Figure 3.3 Simple Agitation Tank Configuration

When fluids with low viscosity are agitated in cylindrical tanks with a centrally attached impeller, baffles are often fitted to inside wall of the tank in order to prevent solid body rotation and vortices. The baffles provide the axial mixing between the top and bottom of the fluid in the tank. They also enhance the turbulent behavior in the agitation system.

In general, four baffles are used in agitation tanks. Their width is often chosen as equal to one tenth of the tank diameter.

Reynolds Number

Reynolds Number (Re) is a dimensionless number used in fluid mechanics. It gives a measure of the ratio of inertial forces to viscous forces to determine the flow regime. It helps to identify the flow as laminar, transitional or turbulent.

For stirred tanks, flow is laminar when Re is lower than 50. Flow is transitional between 50 and 5000, and flow is considered turbulent when Re is higher than 5000.

Reynold's number for non-Newtonian fluids which obey Power Law can be calculated using the below equations 1 to 4:

$$\mathrm{Re} = (\mathrm{B}^{*})^{1-\mathrm{m}} \frac{\mathrm{N}^{2-\mathrm{m}} \mathrm{D_i}^{2} \rho}{\mathrm{n}} \tag{1}$$

$$\dot{\gamma} = \mathrm{B}^{*} \cdot \mathrm{N} \tag{2}$$

$$\eta = \mathrm{n} \cdot \dot{\gamma}^{\mathrm{m}-1} \tag{3}$$

$$\mathrm{B}^{*} = 4\pi \tag{4}$$

Froude Number

Froude Number is a dimensionless number describing the formation of surface vortices. The Froude number is important when gravitational effects are significant, as in vortex formation; its influence is hardly detectable in baffled tanks.

$$N_{Fr} = \frac{N^2 D_i}{g} \tag{5}$$

Power Number

Power Number is a dimensionless number used in fluid mechanics. It is defined as the ratio of the forces on the impeller to the inertial forces. It is one of the most widely used design specifications for mixing processes. It depends on impeller size and position in the tank, tank geometry (size and baffles) and Reynolds Number.

$$N_p = \frac{P}{\rho N^3 {D_i}^5} \tag{6}$$

Figure 3.4 shows the relation between Power Number and Reynolds Number for different types of turbine impellers. If the impeller type and dimensions are specified and Reynolds number is calculated, one can estimate the power required using the curves given in the figure.

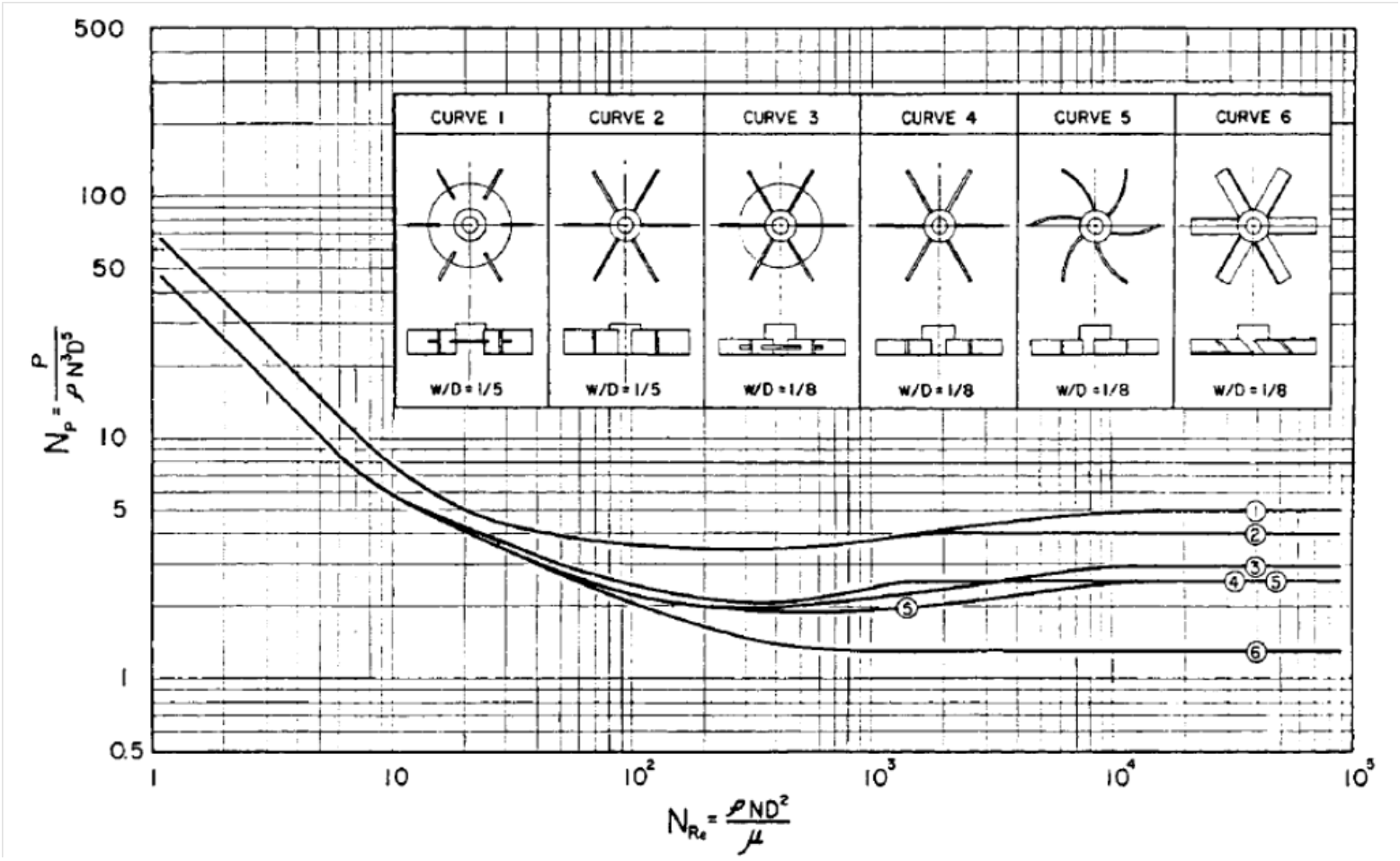

Figure 3.4 Dimensionless Power Number in Stirred Tanks **[22]**

CHAPTER 4

MEASUREMENT TECHNIQUES

In this study, two measurement techniques are adopted. First one is Ultrasound Doppler Velocimetry. It is used to get the velocity profile data inside the agitation tank. The second one is used for mixing time measurement with the help of conductivitymeter.

4.1. Ultrasound Doppler Velocimetry

Ultrasound Doppler Velocimetry is one of the very fast, non-intrusive, and easy to operate methods in order to define flow characteristics.

First appearance of Ultrasound Doppler Velocimeter technique has not been actually in fluid dynamics. In 1980's, UDV techniques is used in medical industry. Combining UDV with pulsed emissions has extended the application area of this technique to other fields and also to fluid dynamics.

One of the significant advantages of UDV is its applicability to both opaque and transparent media. Furthermore, materials from gases to soft solids can be investigated easily in both continuous and batch systems.

Figure 4.1.1 shows the schematic for transducer of UDV system, ultrasonic beam and the particle position.

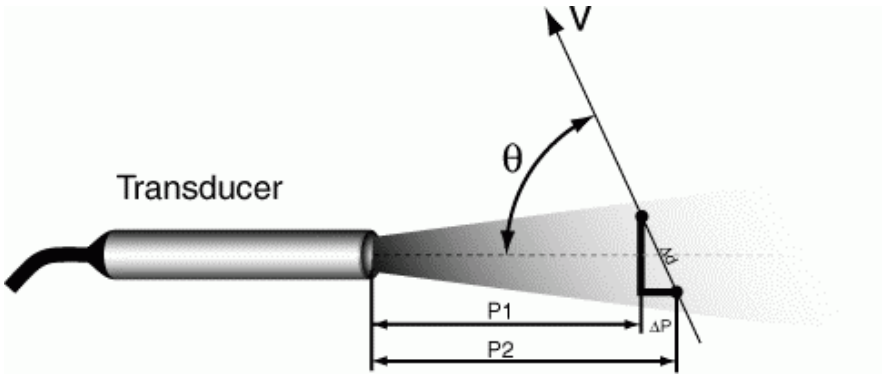

Figure 4.1.1 Moving Particle and Transducer Position **[23]**

Using the time delay T_d between the emitted burst and the echo reflecting back from the particle, the depth p of the mentioned particle can be calculated as:

$$p = \frac{c \cdot T_d}{2} \tag{7}$$

In this equation, c symbolizes the sound velocity of the ultrasonic wave in the liquid. Considering that the particle is moving with an angle θ with respect to the axis of the ultrasonic beam, its velocity can be measured using the variation of the particle's depth between two emissions having time difference T_{prf} **[23]**:

$$P_2 - P_1 = V \cdot T_{prf} \cdot \cos\theta = \frac{c}{2} \cdot (T_2 - T_1) \tag{8}$$

The time difference T_2-T_1 is generally lower than a microsecond. Replacing this time difference by a measurement of the phase shift of the received echo will be easier. So, with f_e is the emitting frequency,

$$\delta = 2\pi \cdot f_e(T_2 - T_1) \tag{9}$$

Then, it can be shown that the velocity of the particle is **[23]**:

$$v = \frac{c \cdot \delta}{4\mu \cdot f_e \cdot \cos\theta \cdot T_{prf}} = \frac{c \cdot f_d}{2 \cdot f_e \cdot \cos\theta} \tag{10}$$

Ultrasound Doppler is capable of providing spatial information associated to velocity values. However, since the data obtained is periodical, UDV technique has the disadvantages stemming from the Nyquist theorem. This means that a maximum velocity exists for each pulse repetition frequency:

$$V_{max} = \frac{c}{4 \cdot T_{prf} \cdot f_e \cdot \cos\theta} \tag{11}$$

This situation causes a limitation in UDV technique: the velocity is limited depending on the pulse repetition frequency. In addition to the velocity limitation, there is also a depth limitation. The ultrasonic burst travels in the liquid at a velocity depending on the physical properties of the liquid. The pulse repetition frequency gives the maximum time allowed to the burst to travel to the particle and back to the transducer **[23]**. The relation between the maximum measurable depth and pulse repetition frequency is:

$$P_{max} = \frac{T_{prf} \cdot c}{2} \tag{12}$$

Thus, maximum measurable depth is related to maximum allowable velocity with the equation:

$$P_{max} V_{max} = \frac{c^2}{8 \cdot f_e \cdot \cos\theta} \tag{13}$$

In this case, although highest emitting frequency gives the best spatial resolution, it may not allow measuring the desired maximum velocity at the maximum depth. So, choosing the optimum emitting frequency should be the first thing before using the UDV technique. Then, the probe diameter should be selected (**APPENDIX A**). While choosing the optimum diameter, it should be noted that smaller diameter means a less sensitive probe and larger diameter means a less diverging beam, i.e. a smaller sampling volume **[23]**.

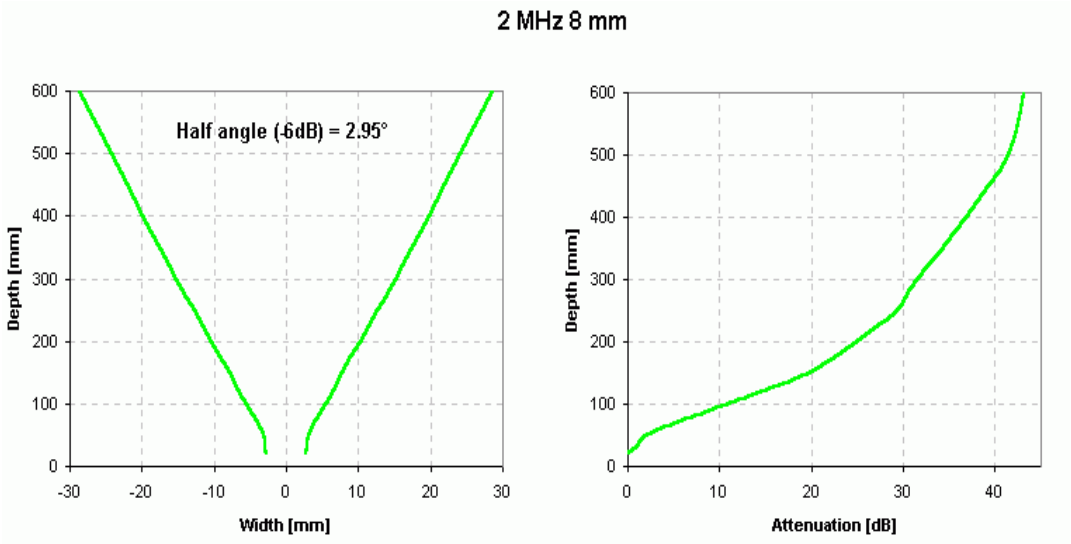

Figure 4.1.2 Beam and attenuation plots of 2 MHz and 8 mm probe **[23]**

Figure 4.1.2 shows the probe specifications used in the study. Depth and width relation of the ultrasonic beam is given. Also, the relation between the attenuation of the beam and penetration depth is given. This plots shows that when the penetration depth increases, volume of the beam also increases causing higher attenuation.

4.1. Conductivity Measurements

Conductance method is one of the mostly applied methods to get the mixing time of the agitated systems. It depends on measuring the conductance of the solution after adding a conductance changing tracer to the initial solution. A conductivitymeter is

used for this kind of measurements. It is important that the instrument gives and records the time dependency of the conductance.

After obtaining the conductance data, it should be combined with conductance and tracer concentration plots. Using these plots, the time for reaching the equilibrium concentration of tracer gives the mixing time of the solution. Generally, 95% of the equilibrium tracer concentration is accepted as the achievement of complete mixing.

CHAPTER 5

EXPERIMENTAL PROCEDURE

The experiments have started with the preliminary viscosity measurements for different concentrations of carboxymethyl cellulose solutions.

5.1. Materials

- Carboxymethyl cellulose (CMC) is the main chemical used throughout this study. It is a cellulose derivative with pseudoplastic (shear thinning) property. It has variable molecular weight and formula (**Figure 5.1.1**). It is often used as its sodium salt, sodium carboxymethyl cellulose. CMC is preferred because it is non-toxic, non-allergenic, environmentally friendly chemical and constituent of many non-food products: toothpaste, artificial eye-drops, water-based paints, detergents, paper products, etc.

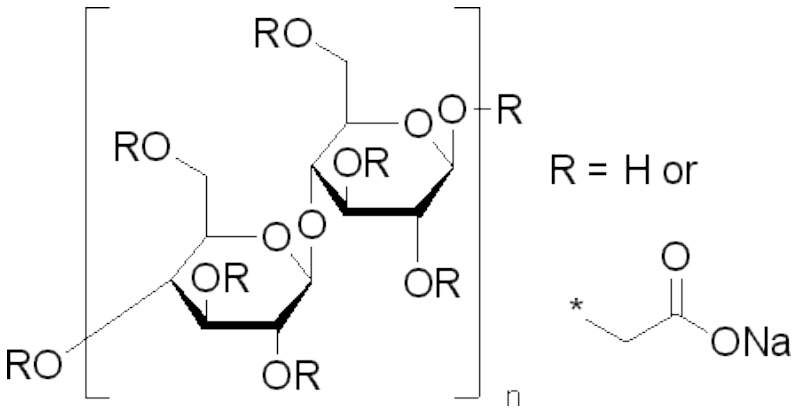

Figure 5.1.1 Structure of CMC **[24]**

CMC is non-toxic, non-allergenic, environmentally friendly chemical. It can be biodegraded aerobically and anaerobically by bacteria commonly found in the environment.

In food industry, CMC is known as E466 and used as viscosity modifier/ thickener or emulsion stabilizer. It is also a constituent of many non-food products: toothpaste, artificial eye-drops, water-based paints, detergents, paper products, building material additives, printing inks, coatings etc as water retention agent, gelling, emulsifying, suspending, absorbing, stabilizing, bonding and film forming agent. For this study, high viscosity Na-CMC salt obtained from Sigma-Aldrich is used.

Sodium chloride is another chemical used in this study. It is used as the electrolytic tracer during the conductivity measurements. The obtained conductivity versus NaCl concentration plots are used to calculate the concentration of NaCl in the viscoelastic solution.

All the measurements have been performed in a cylindrical tank made of plexiglas with a free-surface. The tank included four equally spaced baffles. The tank is filled with CMC solution up to height H.

The impeller is a six-blade Rushton turbine with $D_i = D_t/2$ (**Figure 5.1.3**). The turbine was located with a clearance of H/3 from the bottom of the tank. The impeller is driven by a variable speed electric motor shown in **Figure 5.1.2.**

Figure 5.1.2 Servodyne Mixer Controller and Motor Head

The dimensions of the set-up are given in **Table 5.1.1.**

Table 5.1.1 Agitation Tank and Impeller Dimensions

Diameter of the mixing tank	100 mm
Water height	100 mm
Length of the baffles	120 mm
Thickness of the baffles	2 mm
Width of the baffles	10 mm
Diameter of the mixer shaft	9 mm
Impeller clearance	33 mm
Impeller diameter (2”)	51 mm
Disc diameter	30 mm
Disc thickness	2 mm
Bore diameter (⅜”)	10 mm
Blade length	10 mm
Blade thickness	2 mm

Figure 5.1.3 Rushton Turbine and the Impeller

The cylindrical vessel is placed in water-filled square tank made of plexiglass to prevent the attenuation of ultrasonic beams. Twenty five holes are drilled on the square tank's surface in order to place the UDV probe. The set-up is showed in **Figure 5.1.4, Figure 5.1.5** and **Figure 5.1.6.**

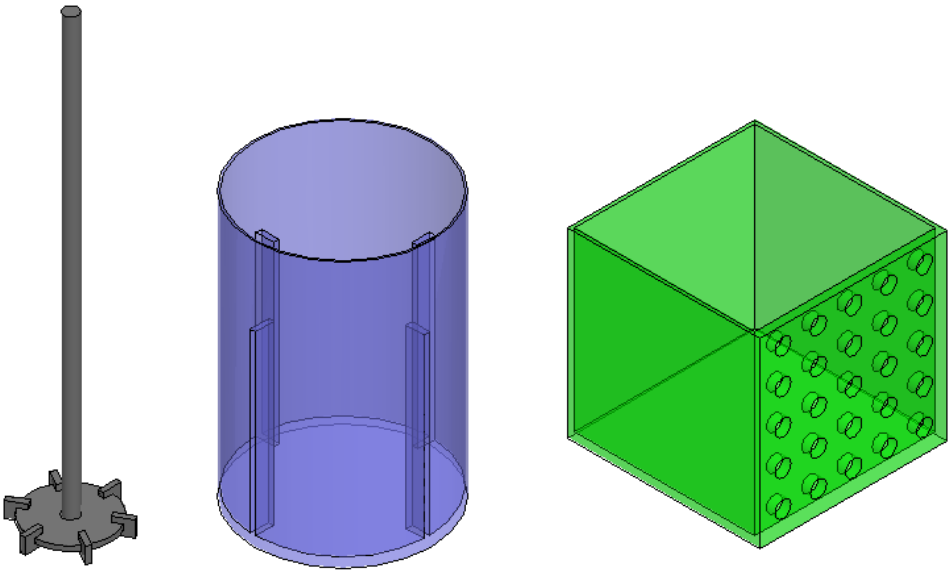

Figure 5.1.4 The Parts of the Tank Set-up: Rushton turbine with the shaft, cylindrical tank with baffles, square tank with holes (from left to right)

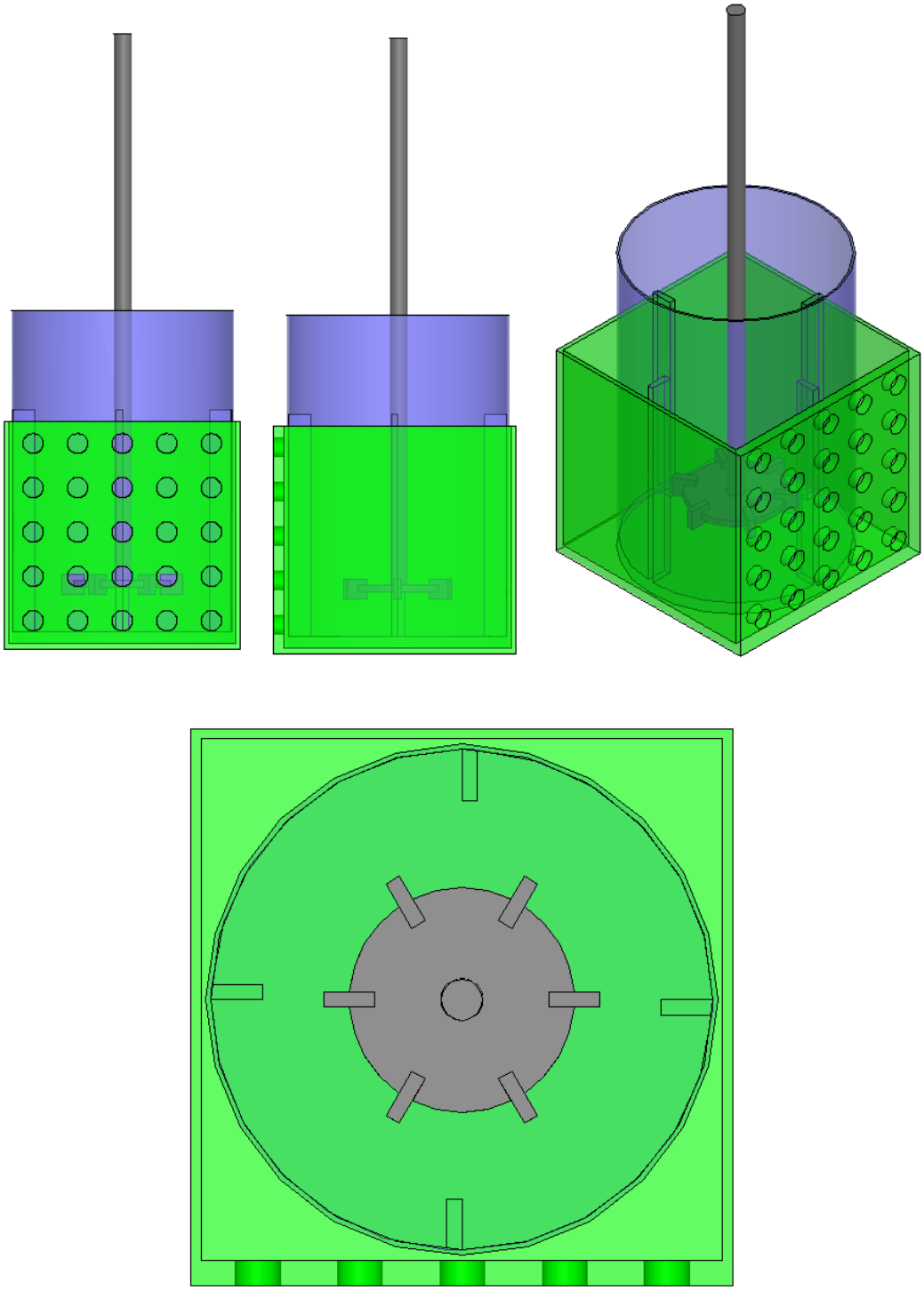

Figure 5.1.5 Arrangement of the Tank Set-up with Sectional Views

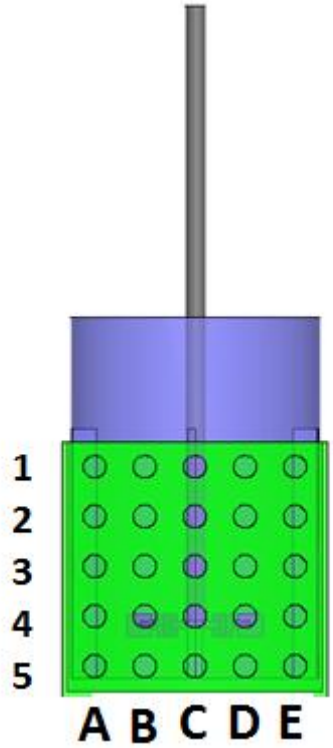

Figure 5.1.6 Grid Prepared for Probe Positions

5.2. Methodology

Solution Preparation

Solutions are prepared by mixing distilled water and carboxymethyl cellulose at different percentages. After addition of CMC in distilled water, the mixture is stirred vigorously until the homogeneity is achieved. Then, solutions are used for viscosity measurement, velocity profiling and mixing time measurements.

Viscosity Measurements

The viscosities of the CMC solutions prepared with different concentrations have been measured with Brookfield DVIII Ultra rheometer in terms of the shear rates

(**Figure 5.2.1**). Spindle number 34 (accessory of the mentioned rheometer) has been used during the experiments. The viscosity measurements have been performed at 20°C.

Figure 5.2.1 Brookfield DV-III Ultra Rheometer

Velocity Profile Measurements

To find the velocity profile in the cylindrical tank, DOP2000 Ultrasound Doppler Velocimeter (designed by Signal Processing SA) has been used (**Figure 5.2.2**). To complement the velocimeter, the 2 MHz transducer with 8 mm diameter has been chosen and used (**Figure 5.2.3**). 128 profiles have been recorded for each point on the measurement grid.

Before the probe is placed in the holes of the grid, its piezoelectric tip is covered with ultrasonic gel to enhance the contact surface. Furthermore, carboxymethyl cellulose solution is filled between the inner cylindrical tank and outer rectangular tank as a coupling solution. Obtained raw data is analyzed after mean velocities are computed.

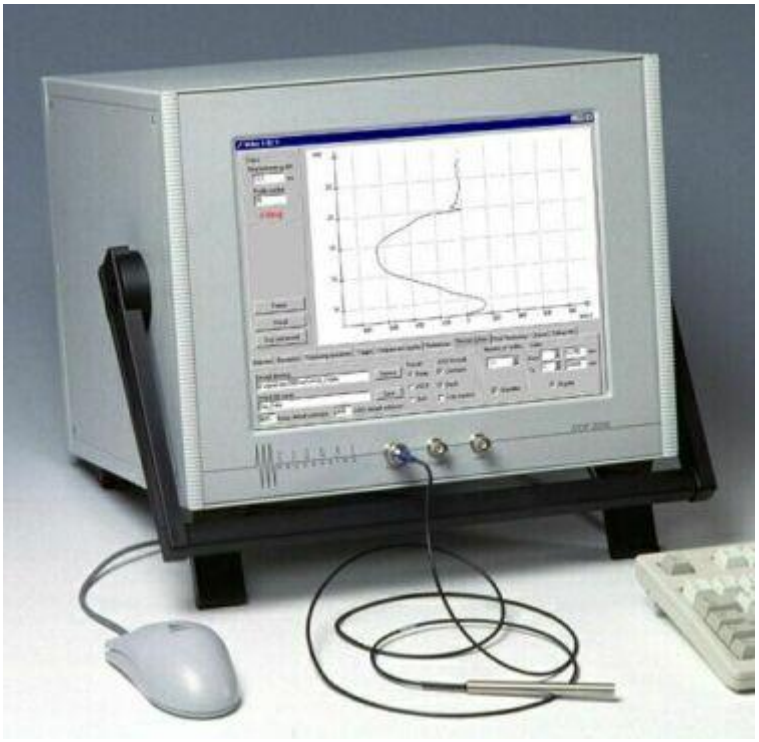

Figure 5.2.2 Stand-alone Integrated DOP2000 Velocimeter **[23]**

Figure 5.2.3 UDV Probe

Mixing Time Measurements

Mixing time measurements were carried out by adding NaCl solution instantaneously and monitoring the conductance of the mixture in the tank at a certain location using a conductivity probe. 0.1 M salt solution (NaCl) is used as the tracer. 8 ml (corresponding to 0.1% of the volume of CMC solution in the tank) of the NaCl solution was injected inside the tank near the shaft. The mixing time was calculated as the time required for the salt concentration to reach 95% of the equilibrium salt concentration corresponding to the final conductance of the solution.

Power Consumption

In industrial mixing applications, following the power consumption of agitation systems is very important. In spite of its widespread use, the dependence of power consumption on impeller and tank geometry can be defined only in the most general terms. This is partly due to the difficulty of obtaining accurate torque measurements on the small scale and partly due to the predictive limitations of drag theory, particularly for the recirculating three dimensional flows **[26]**.

Correlations for Power Number and Reynolds Number are used to calculate power consumption of the systems under investigation. An efficient impeller in terms of power consumption should have a small mixing time and a small power number.

Power consumption of the system can be computed according to the equations given below **[14]**.

$$N_p = \frac{P}{\rho N^3 D^5} \tag{14}$$

$$P = 2\pi N T_q \tag{15}$$

$$N_p = \frac{2\pi T_q}{\rho N^2 D^5} \tag{16}$$

$$T_q = \int_0^{\frac{D}{2}} F_D \, dr = \int_0^{\frac{D}{2}} C_D \rho \frac{V^2}{2} hr \, dr \tag{17}$$

$$= C_D \rho h \pi^2 N^2 \int_0^{D/2} r^3 \, dr \; \propto \; \rho N^2 D^5 \tag{18}$$

CHAPTER 6

RESULTS AND DISCUSSION

The results have been evaluated in several sub-sections. Viscosity measurement, velocity profile characterization, effect of various parameters on velocity profile, mixing time and power consumption are analyzed separately.

6.1. Viscosity Characterization of the CMC Solutions

CMC solutions with varying concentrations have been prepared and their viscosities have been measured via the rheometer. At the end, it is seen that 0.5 wt %, 1 wt% and 2 wt% CMC solutions will be enough for the remaining part of the study. In **Figure 6.1.1,** the shear thinning nature of the prepared CMC-water solutions is easy to notice. As expected, viscosity decreases with increasing shear rate. This situation is due to the disentanglements of the long molecule chains under pressure. Also, even with very low percentages, high viscosities can be reached.

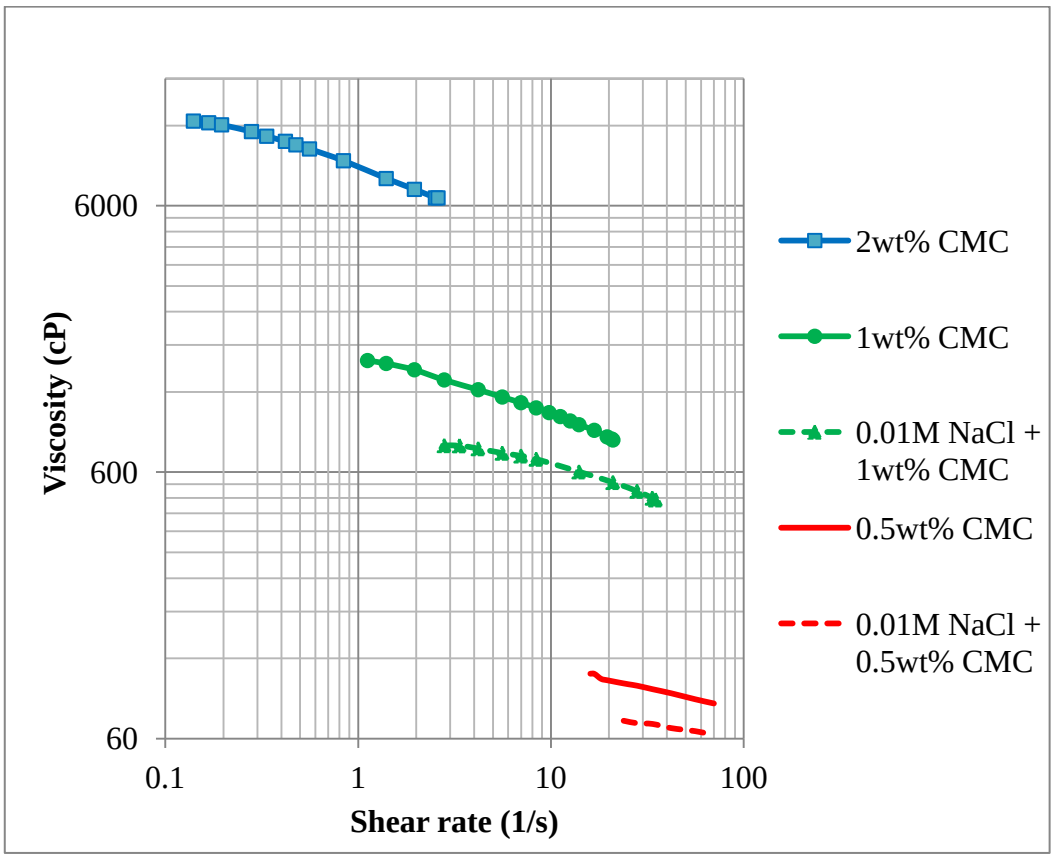

Figure 6.1.1 Viscosity of CMC solutions

6.2. Effects of Salt Concentration on Solution Viscosity

Figure 6.2.1 and **Figure 6.2.2** show the effect of electrolytic tracer on the solution viscosity. It is observed that electrolytic tracer decreases the viscosity.

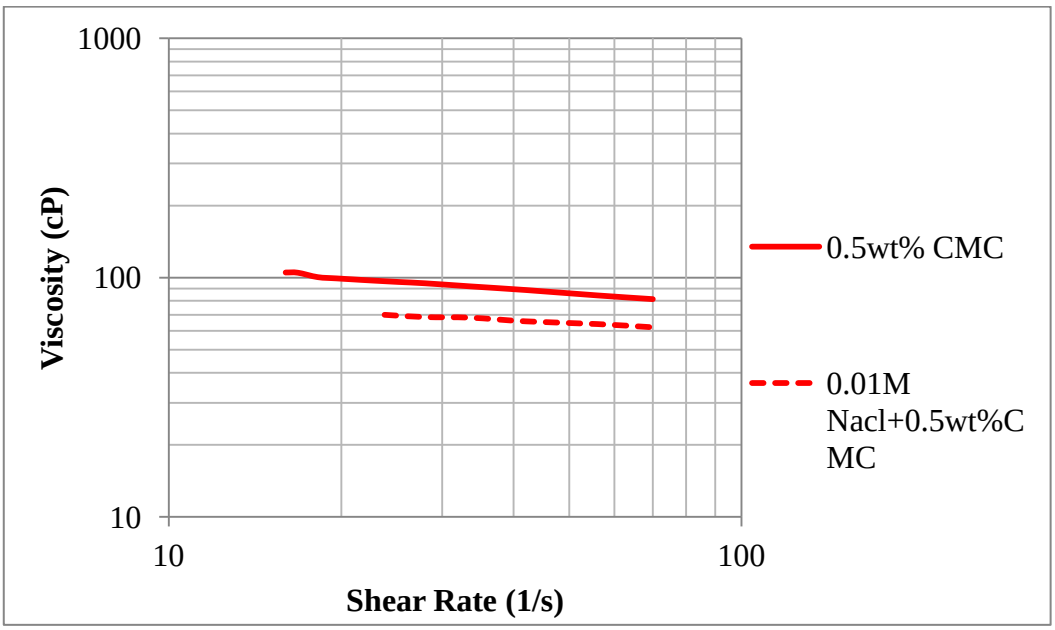

Figure 6.2.1 Effect of Electrolyte Addition on the Viscosity of CMC Solution

From the Figure 6.2.1, we can see that NaCl addition decreases the viscosity of CMC solution approximately 24%.

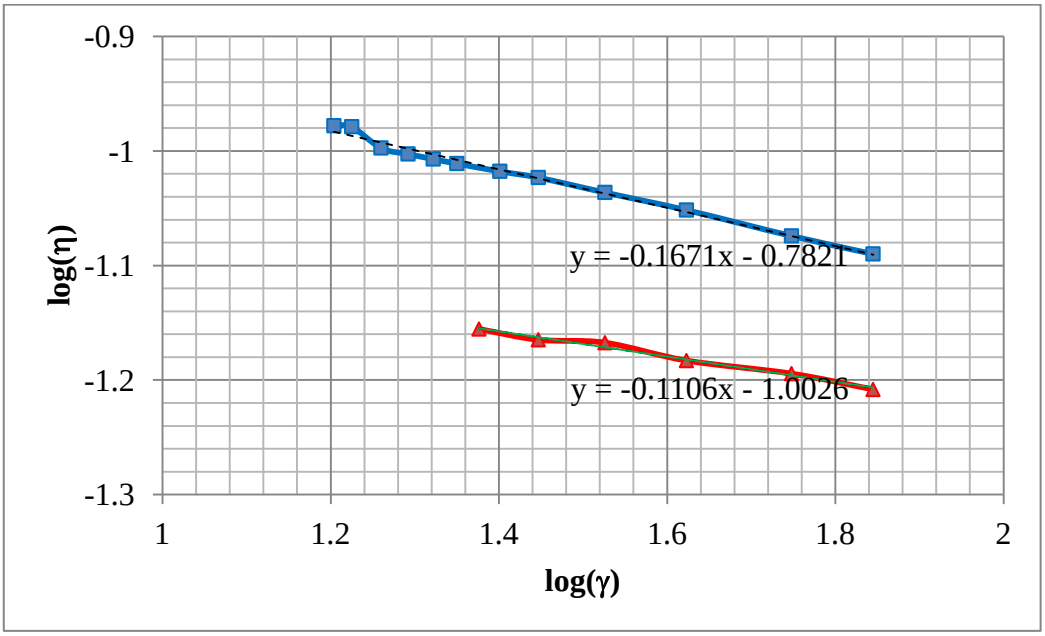

Figure 6.2.2 Effect of Electrolyte Addition on the Viscosity of CMC Solution

Figure 6.2.2 shows also the Power Law indices of shear-thinning for 0.5wt% CMC solution:

$$\eta = n\,\gamma^{m-1} \tag{19}$$

$$\log\eta = \log n + (m-1)\log\gamma \tag{20}$$

$\log\eta = -0.7821 - 0.1671\log\gamma$ (without NaCl)

$\rightarrow$ n=0.1652 Pa.s^m m=0.8329

$\log\eta = -1.0026 - 0.1106\log\gamma$ (with NaCl)

$\rightarrow$ n=0.0994 Pa.s^m m=0.8894

Table 6.2.1 shows the calculated Power Law indices of the CMC solutions used in the experiments with different concentrations.

Table 6.2.1 Power Law Indices

CONCENTRATION	**EQUATION**	**n (Pa.s^m)**	**m**
0.5 wt % CMC	$\log\eta$ = -0.1671 $\log\gamma$ - 0.7821	0.1652	0.8329
1 wt % CMC	$\log\eta$ = -0.2372 $\log\gamma$ + 0.228	1.6904	0.7628
2 wt % CMC	$\log\eta$ = -0.2396 $\log\gamma$ + 0.9166	8.2528	0.7604

6.3. Effect of Position on Velocity Profile

Twenty five positions on the grid have been used for velocity measurements. The probe of UDV is used to obtain the spatial velocity distribution along the measurement axis.

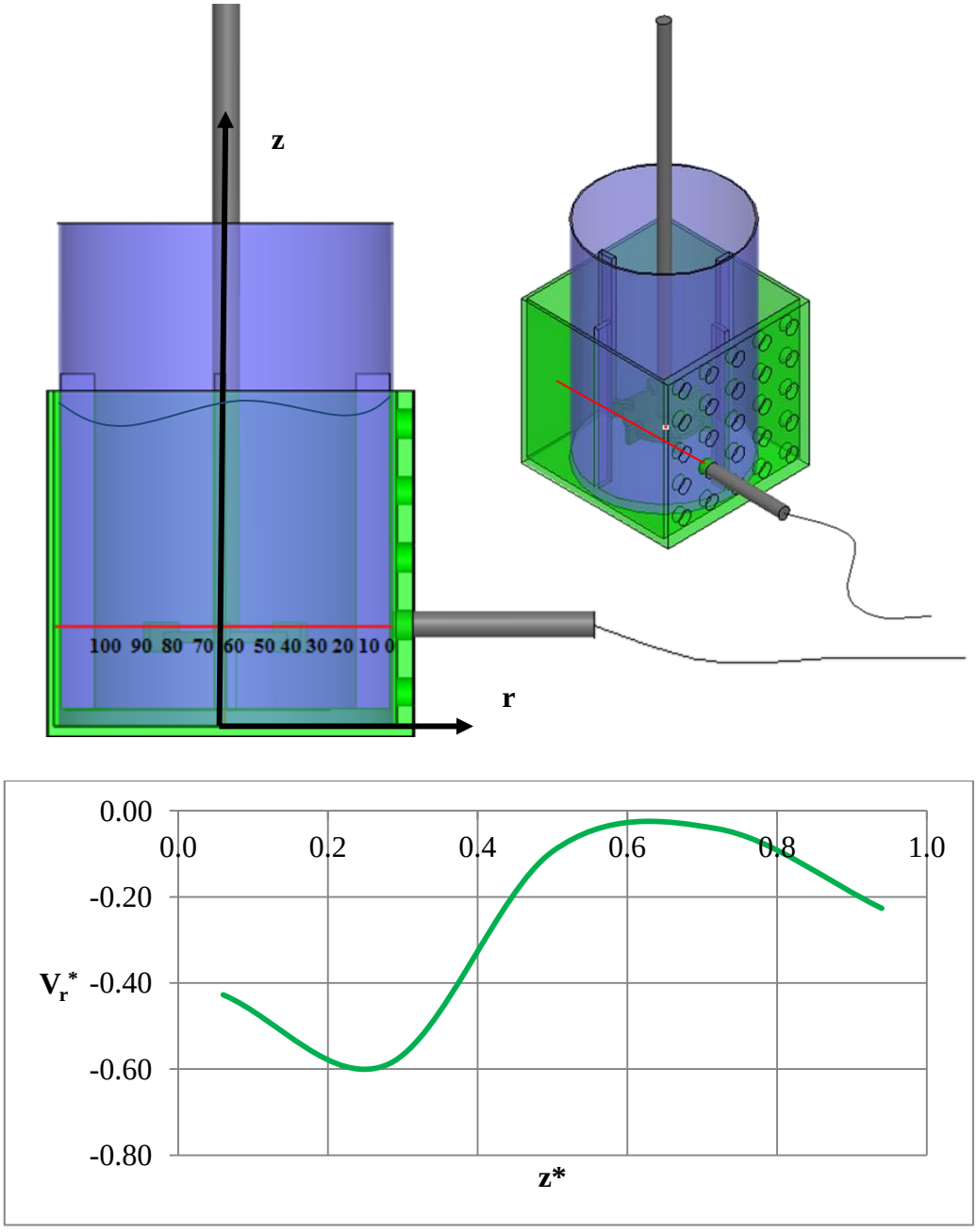

Figure 6.3.1 Sample Velocity Measurement along the z-axis for 1 wt% CMC Solution at 150 rpm at 100 mm away from Probe Tip

Figure 6.3.1 shows a sample measurement along the z-axis changing probe location from B1 (top of the tank) up to B5 (bottom of the tank). In this figure and also in the velocity results presented in this section, dimensionless distances are used to give the velocity component. These are defined below with respect to impeller tip velocity and tank height:

$$V_r^* = V_r/U_{tip}$$

$$V_t^* = V_t/U_{tip}$$

$$z^* = z/(H*1000)$$

Figure 6.3.2 illustrates the radial velocity distribution sample at 60 mm away from the probe tip (i.e. impeller region). From this figure, it can be concluded that error bars are in the range of 3-7% of the average values. The errors for velocity profiles at the top and bottom of the tank are greater than the errors for velocity profiles near the impeller region. However, for all the study, maximum error ranges were not greater than 7% of the average values. Thus, the velocity profile characterization identified in this study gives repeatable results.

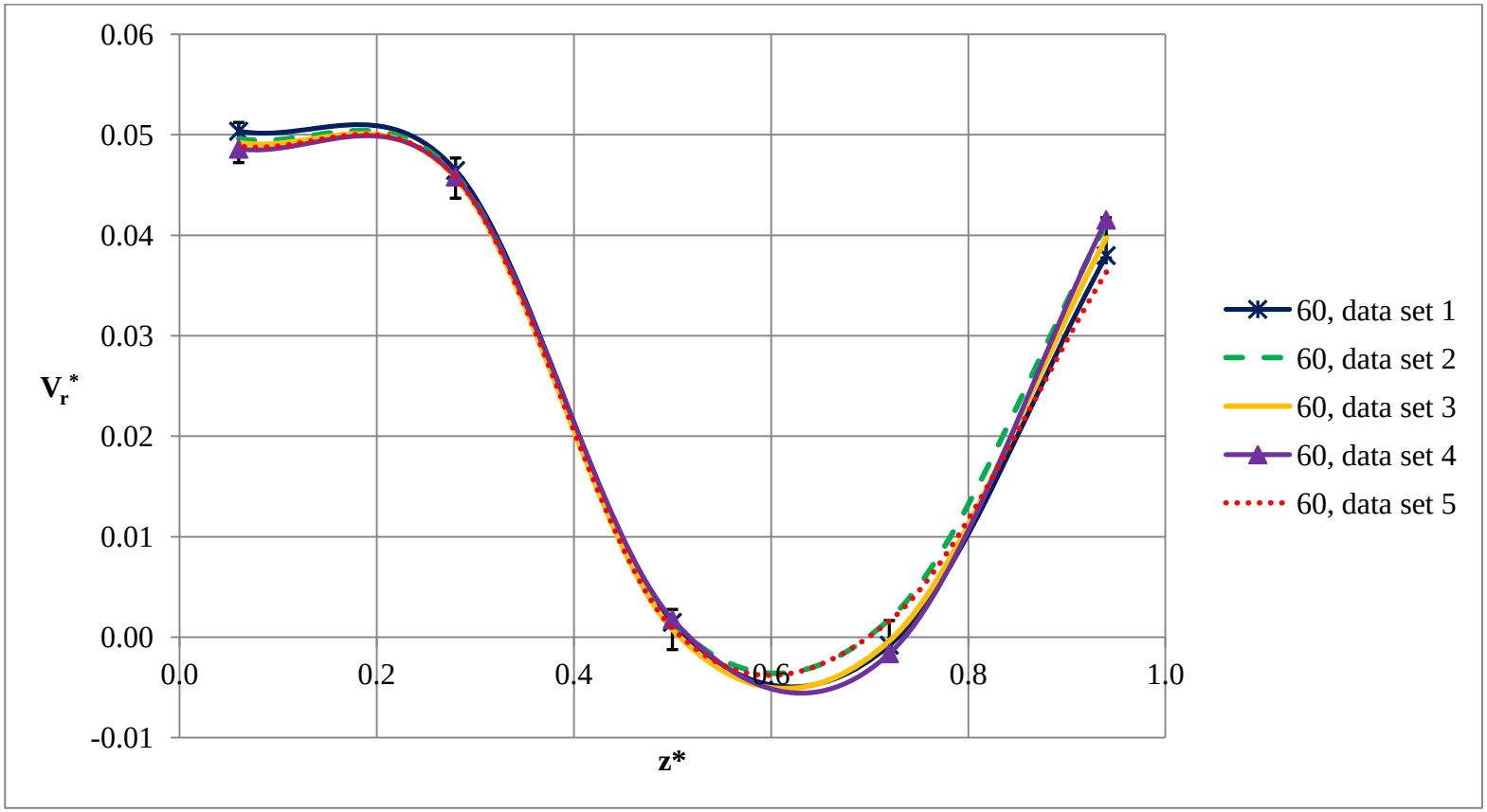

Figure 6.3.2 Velocity Distribution at B Line for 1 wt% CMC Solution at 150 rpm at 60 mm away from Probe Tip

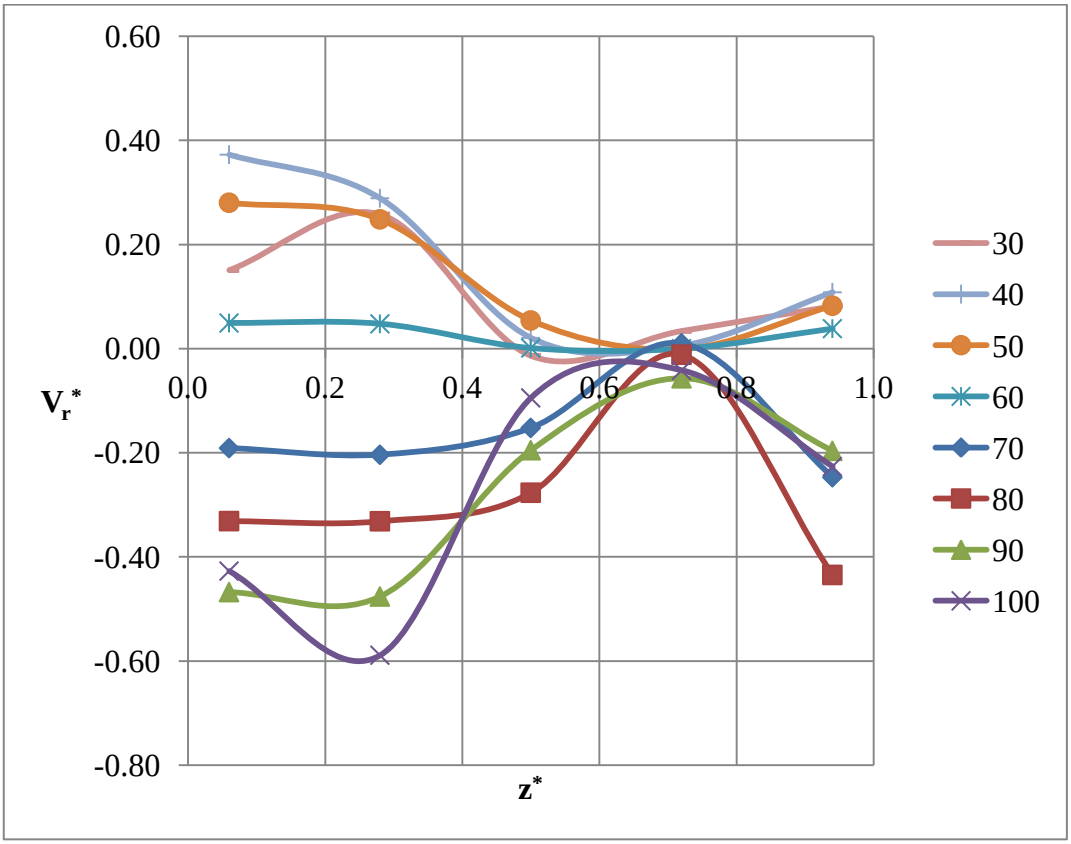

Figure 6.3.3 Velocity Distribution at B Line for 1 wt% CMC Solution with 150 rpm

Figure 6.3.3 shows the radial velocity distribution in the 1 wt% CMC solution along the z-axis at B line direction with impeller speed at 150 rpm at different positions with respect to distance to probe tip. The velocity is given at different lines in terms of their distance to probe. The line named as "30" is the nearest point and the line named "100" is the most far point with respect to the probe tip. The shaft of the impeller is between the lines "60" and "70". The impeller is placed at the point 0.3 axially. Thus, we can conclude from this figure that radial velocity reaches the highest value near the impeller region and it is also higher around walls of the tank. Around the axial point "0.7", the radial velocity reaches its minimum, and then it increases a little bit. This situation may be due to the "two compartments" phenomena occurring with radial flow impellers.

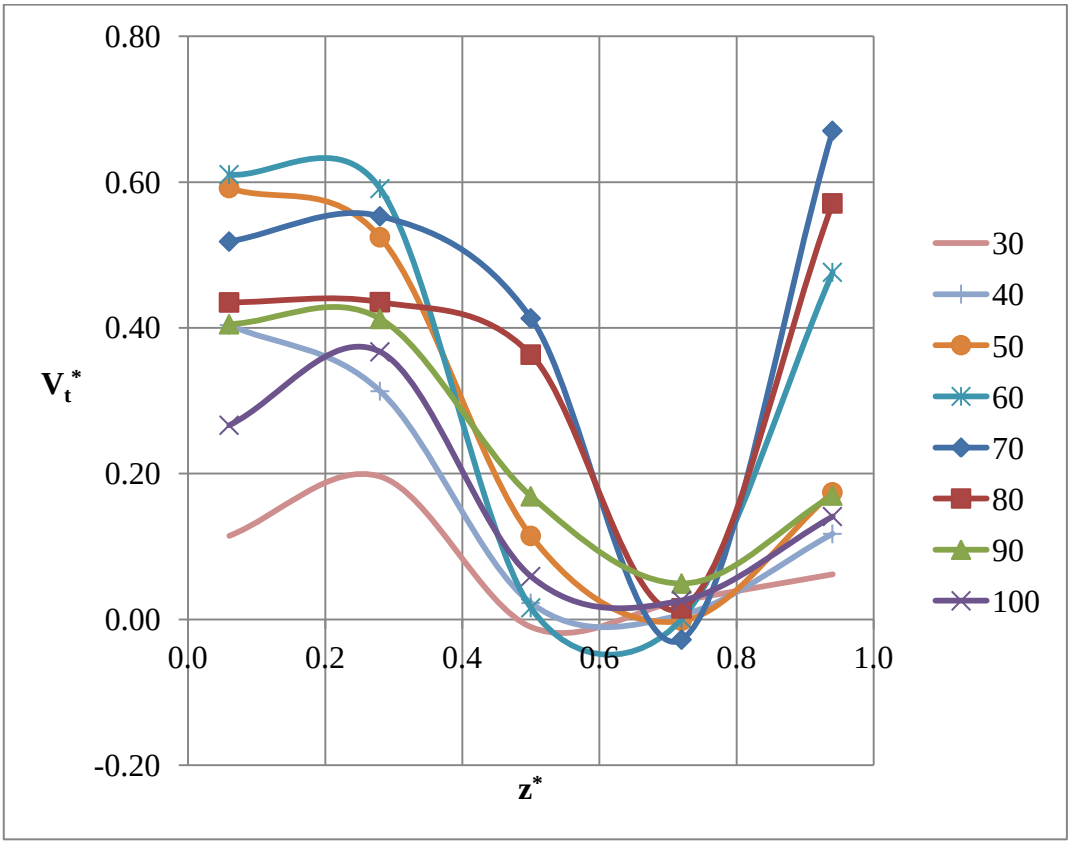

Figure 6.3.4 Velocity Distribution at B Line for 1 wt% CMC Solution with 150 rpm

Figure 6.3.4 shows the tangential velocity distribution in the 1 wt% CMC solution along the z-axis at B line direction with impeller speed at 150 rpm. The velocity is given at different lines in terms of their distance to probe tip. The impeller is placed at the point 0.3 axially. Thus, we can conclude from this figure that tangential velocity reaches the highest value near the impeller region and it is also higher around impeller shaft. The theoretical value of tip velocity of the impeller is 400 mm/s. The figure shows that measured tip velocity around the impeller is almost 62.5% (250 mm/s) of the theoretical value. This difference may be due to losses stemming from the viscous forces. Around the axial point "0.7", the tangential velocity reaches its minimum, and then it increases. This situation may be due to the "two compartment" phenomena occurring with radial flow impellers.

The velocity measurements for the other probe positions and conditions are given in **APPENDIX B**. Considering all the results presented in this section, velocity is higher in the regions around the impeller and it is lower around walls, at the tank of the bottom and at the top of the tank. As expected, increasing CMC solution concentration decreases the ratio of the measured speed to theoretical speed due to increasing viscosity. However, it can be said that shear-thinning nature of the CMC solutions affects the ratio of measured velocity to theoretical velocity: when the impeller speed gets higher, this ratio seems to increase.

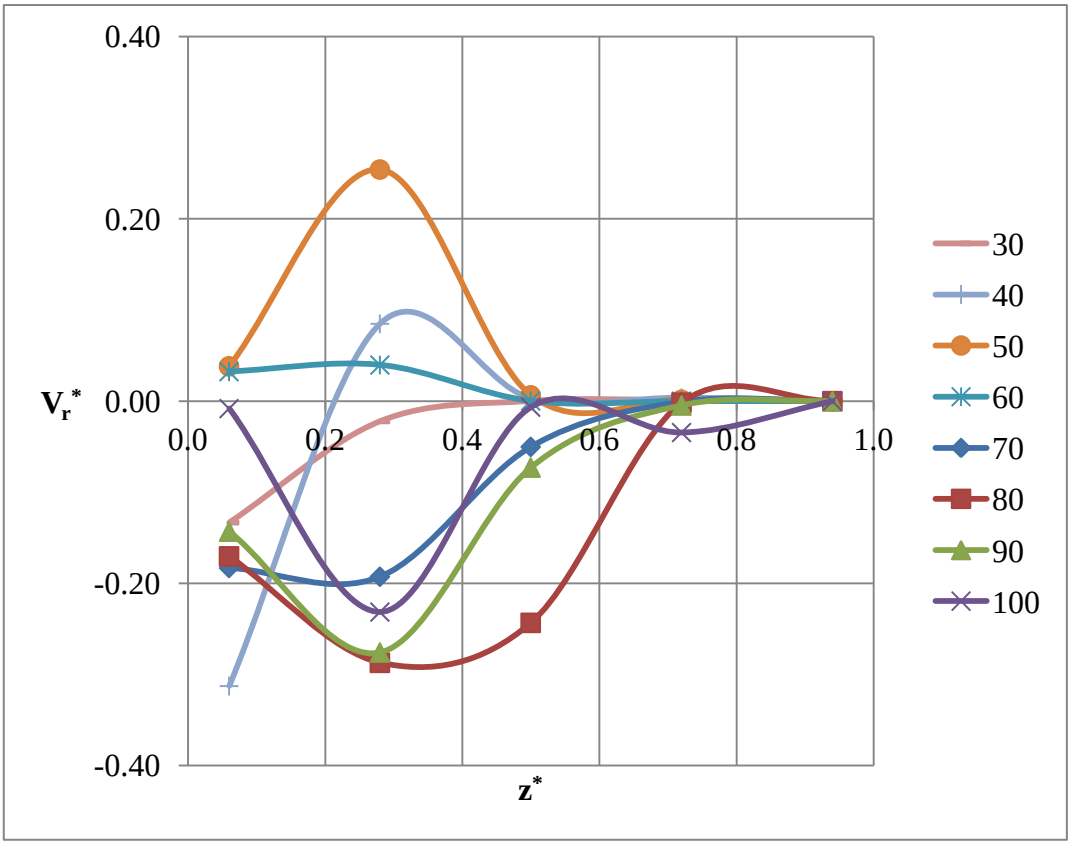

Figure 6.3.5 Velocity Distribution at B Line for 0.5 wt% CMC Solution with 600 rpm

Figure 6.3.5 shows the radial velocity distribution in the 0.5 wt% CMC solution along the z-axis at B line direction with impeller speed at 600 rpm. The velocity is given at different lines in terms of their distance to probe. We can conclude from this figure that radial velocity reaches the highest value near the impeller region and

it is also higher around walls of the tank. Around the axial point “0.7”, the radial velocity reaches its minimum, and then it increases a little bit. This situation may be due to the “two compartments” phenomena occurring with radial flow impellers.

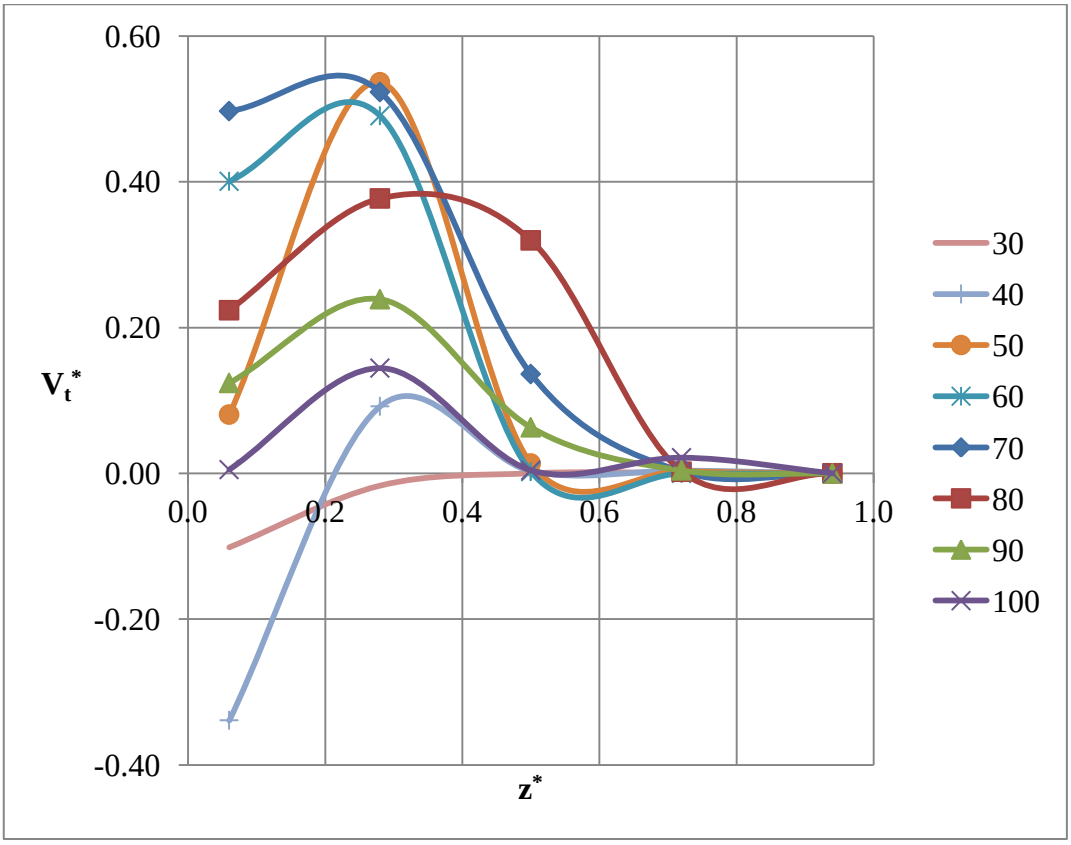

Figure 6.3.6 Velocity Distribution at B Line for 0.5 wt% CMC Solution with 600 rpm

Figure 6.3.6 shows the tangential velocity distribution in the 0.5 wt% CMC solution along the z-axis at B line direction with impeller speed at 600 rpm. The velocity is given at different lines in terms of their distance to probe tip. The figure shows that tangential velocity reaches the highest value near the impeller region and it is also higher around impeller shaft. The theoretical value of tip velocity of the impeller is 1600 mm/s. The figure shows that measured tip velocity around the impeller is 52.2% of the theoretical value (835 mm/s). This difference may be due to losses

stemming from the viscous forces. Around the axial point “0.7”, the tangential velocity reaches its minimum, and then it increases.

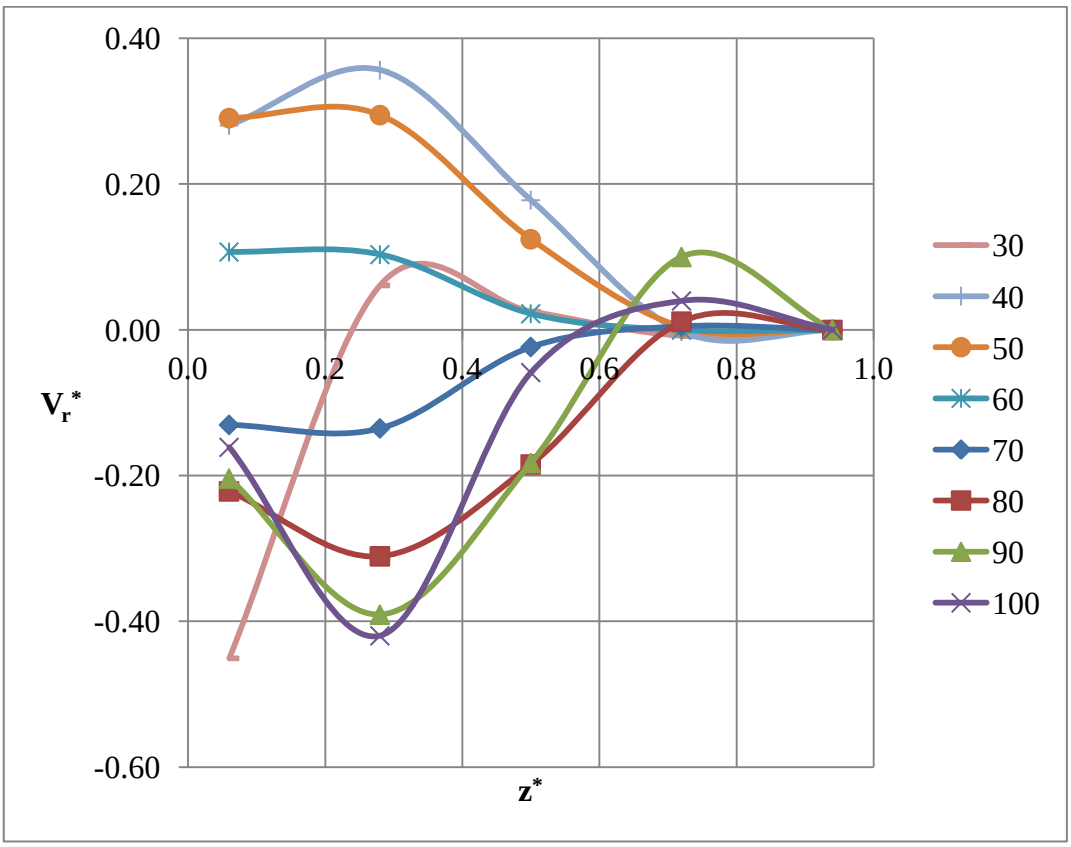

Figure 6.3.7 Velocity Distribution at B Line for 2 wt% CMC Solution with 300 rpm

Figure 6.3.7 shows the radial velocity distribution in the 2 wt% CMC solution along the z-axis at B line direction with impeller speed at 300 rpm. We can conclude from this figure that radial velocity reaches the highest value near the impeller region and it is also higher around walls of the tank. Around the axial point “0.7”, the radial velocity reaches its minimum, and then it increases a little bit.

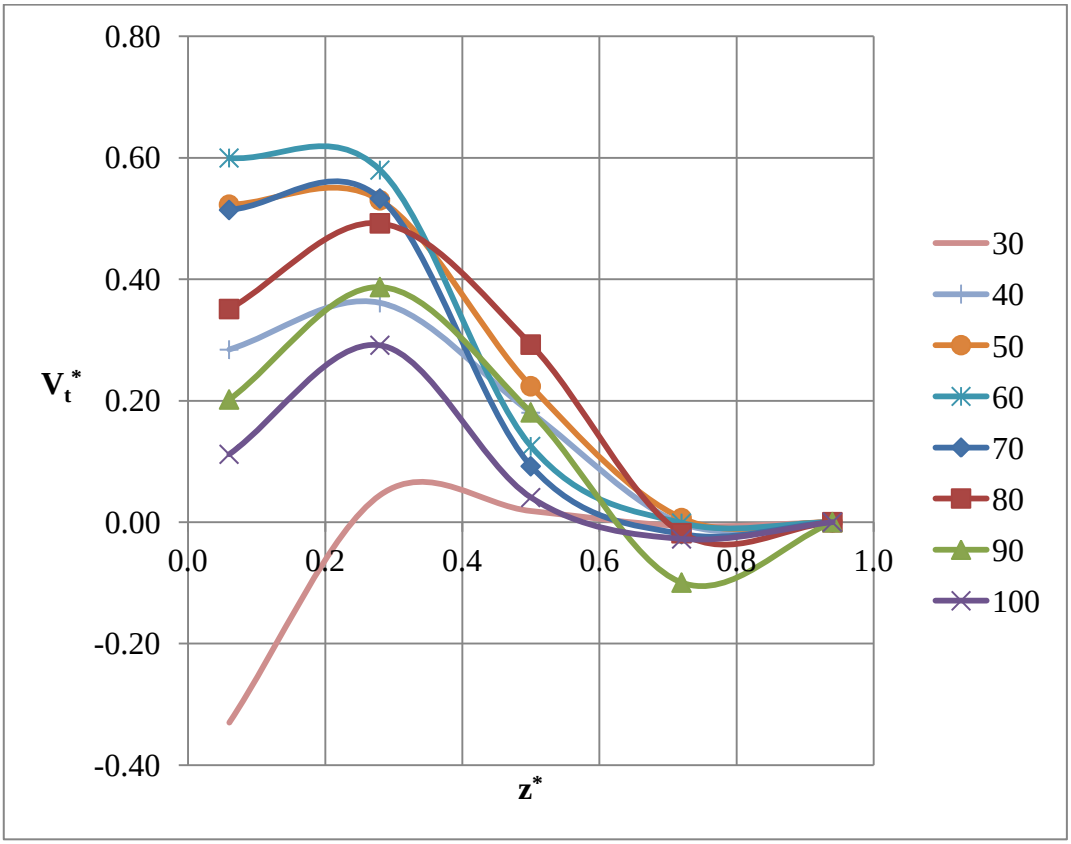

Figure 6.3.8 Velocity Distribution at B Line for 2 wt% CMC Solution with 300 rpm

Figure 6.3.8 shows the tangential velocity distribution in the 2 wt% CMC solution along the z-axis at B line direction with impeller speed at 300 rpm. The theoretical value of tip velocity of the impeller is 800 mm/s. The figure shows that measured tip velocity around the impeller is 58.8% of the theoretical value (470 mm/s).

6.4. Effect of Impeller Speed on Velocity Profile

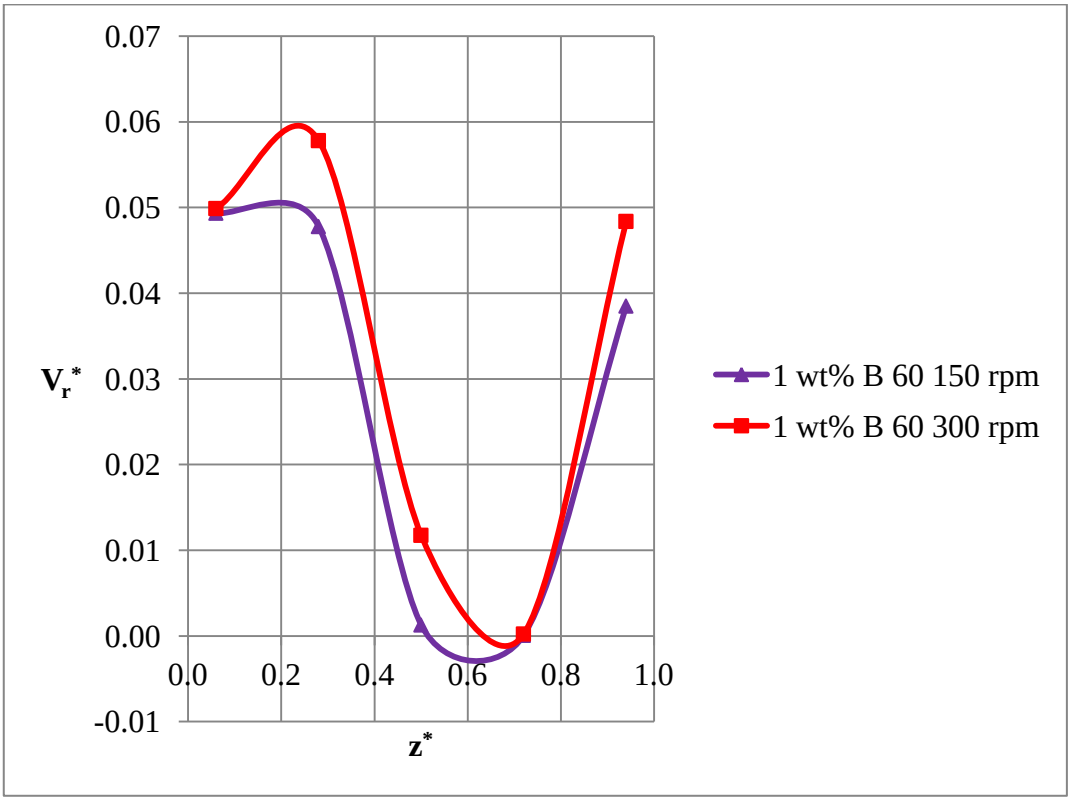

Figure 6.4.1 Effect of Impeller Speed on Velocity Distribution

Figure 6.4.1 shows the radial velocity distribution in the 1 wt% CMC solution along the z-axis at B line direction at different impeller speeds. The impeller is placed at the point 0.3 axially for each case. It can be concluded from this figure that radial velocity reaches the highest value near the impeller region for all three impeller speeds and it is also higher around walls of the tank. Around the axial point "0.7", the radial velocity reaches its minimum. Also, it can be observed that velocity is higher for 300 rpm than 150 rpm.

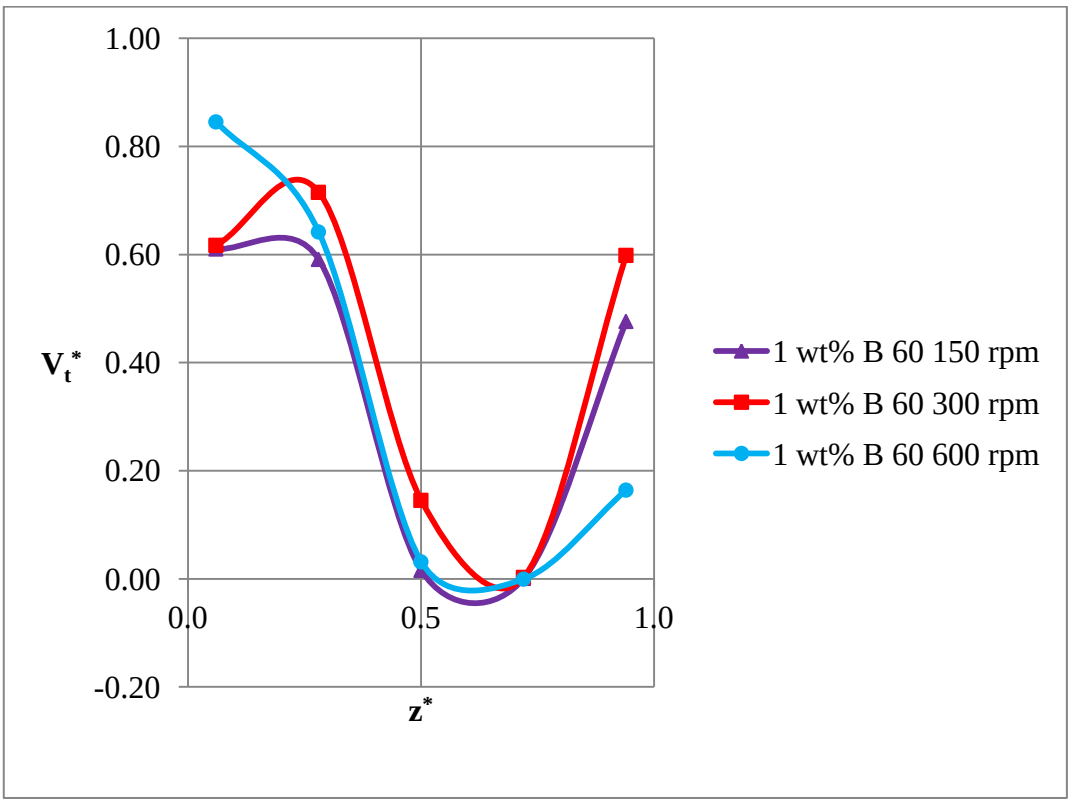

Figure 6.4.2 Effect of Impeller Speed on Velocity Distribution

Figure 6.4.2 shows the tangential velocity distribution in the 1 wt% CMC solution along the z-axis at B line direction at different impeller speeds. The impeller is placed at the point 0.3 axially for each case. Thus, we can conclude from this figure that tangential velocity reaches the highest value near the impeller region and it is also higher around impeller shaft for each case. The figure shows that measured tip velocity around the impeller is approximately 60% of the theoretical value for 150 rpm, 75% of the theoretical value for 300 rpm and 69% of the theoretical value for 600 rpm. Also, velocity is highest for 600 rpm case and it is lowest for 150 rpm case as expected.

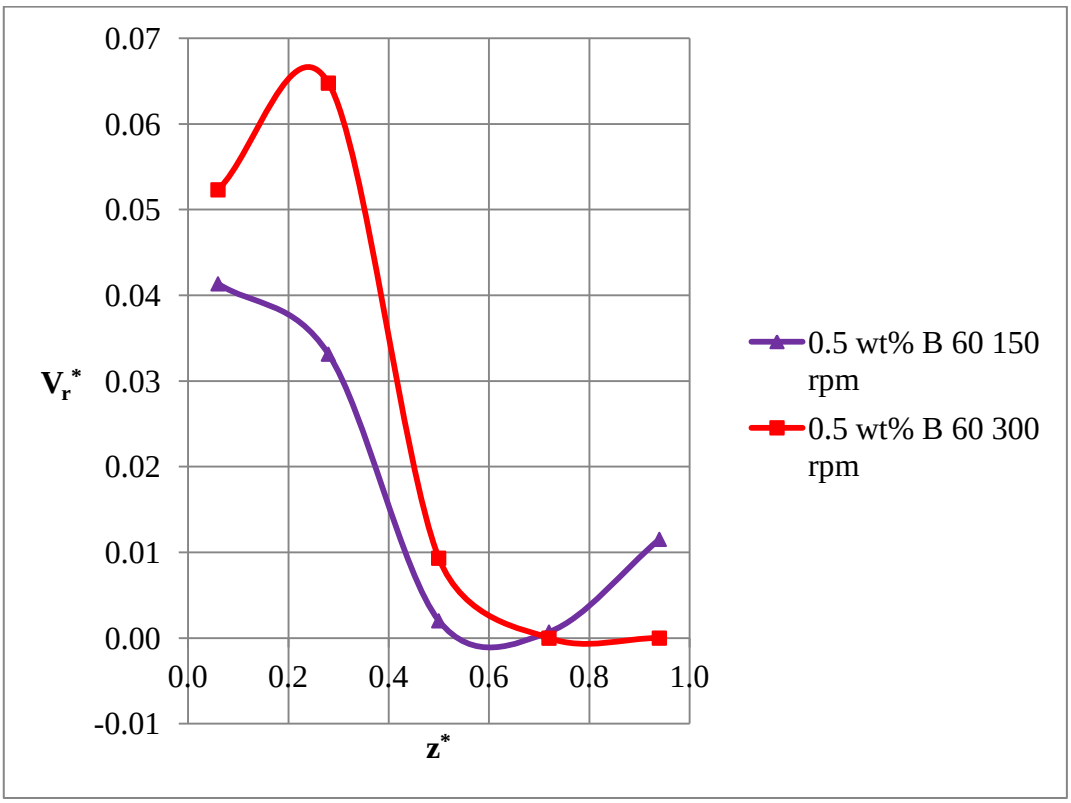

Figure 6.4.3 Effect of Impeller Speed on Velocity Distribution

Figure 6.4.3 shows the radial velocity distribution in the 1 wt% CMC solution along the z-axis at B line direction at different impeller speeds. The impeller is placed at the point 0.3 axially for each case. For both cases, velocity is higher around the impeller. Also, velocity is higher for 300 rpm case than 150 rpm case.

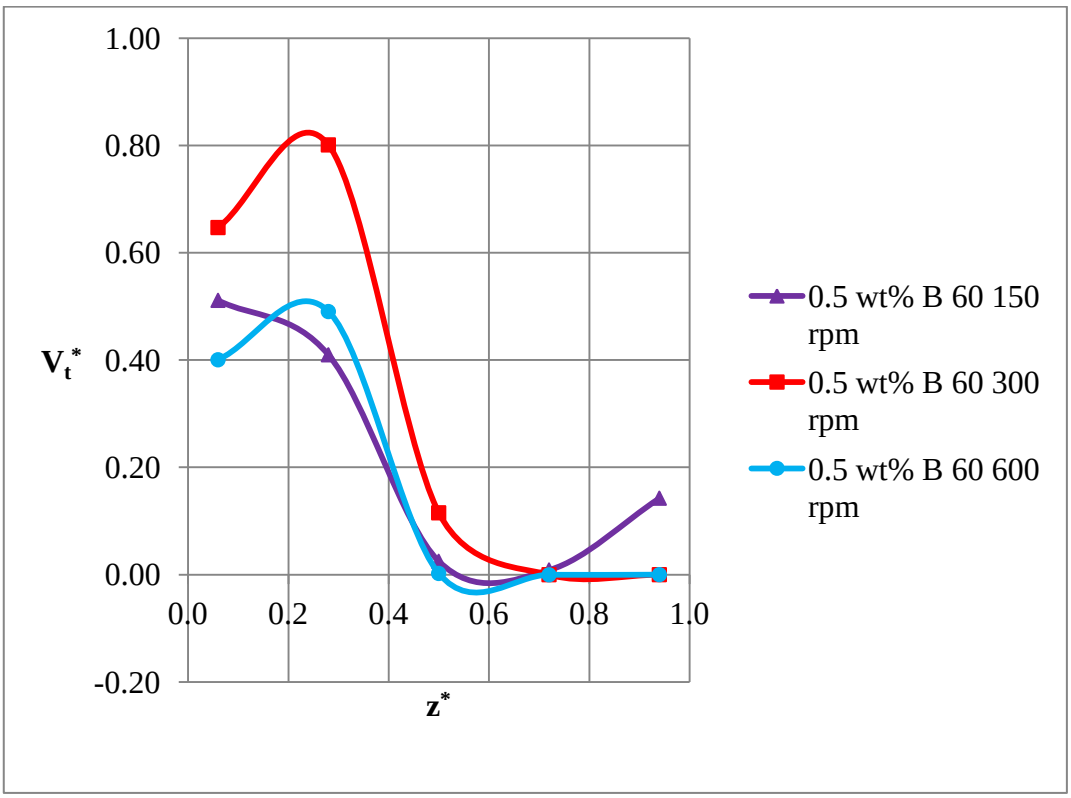

Figure 6.4.4 Effect of Impeller Speed on Velocity Distribution

Figure 6.4.4 shows the tangential velocity distribution in the 0.5 wt% CMC solution along the z-axis at B line direction at different impeller speeds. The impeller is placed at the point 0.3 axially for each case. Thus, we can conclude from this figure that tangential velocity reaches the highest value near the impeller region and it is also higher around impeller shaft for each case. The figure shows that measured tip velocity around the impeller is approximately 43% of the theoretical value for 150 rpm, 80% of the theoretical value for 300 rpm and 51% of the theoretical value for 600 rpm. Also, velocity is highest for 600 rpm case and it is lowest for 150 rpm case as expected.

6.5. Effect of Concentration on Velocity Profile

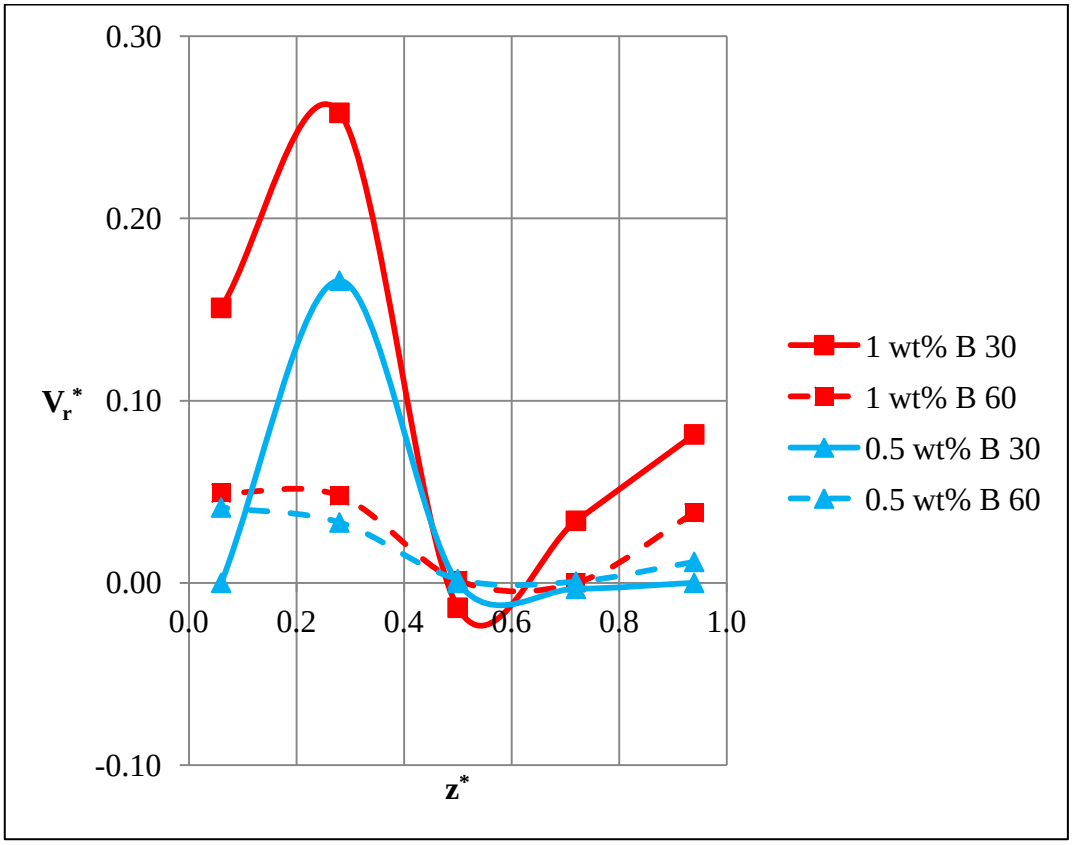

Figure 6.5.1 Effect of CMC Solution Concentration on Velocity Distribution at 150 rpm

Figure 6.5.1 shows the radial velocity distribution in the 0.5 and 1 wt% CMC solution along the z-axis at B line direction with impeller speed at 150 rpm at two different locations. In the figure, it is observed that the radial velocity for 1 wt% CMC solution is higher than the radial velocity for 0.5 wt% CMC solution. Also, interestingly, the velocities are lower near the impeller region than the ones near the tank wall.

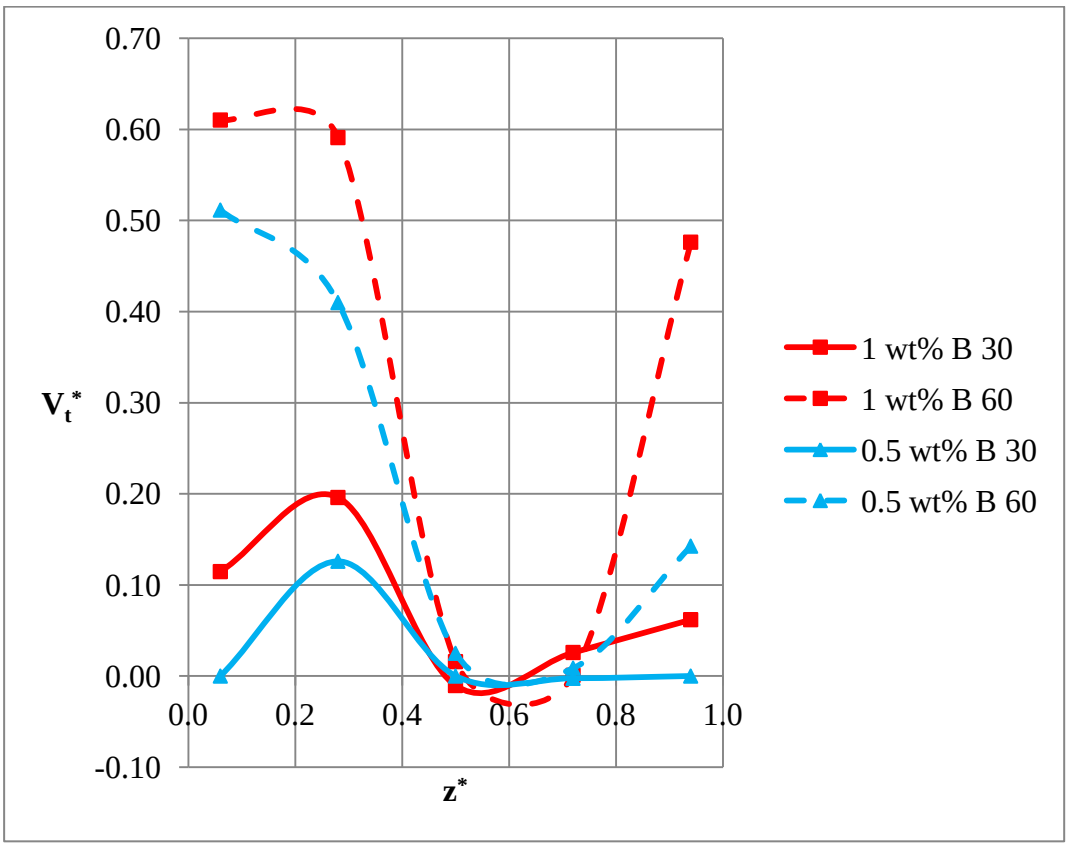

Figure 6.5.2 Effect of CMC Solution Concentration on Velocity Distribution at 150 rpm

Figure 6.5.2 shows the tangential velocity distribution in the 0.5 wt% and 1 wt% CMC solutions along the z-axis at B line direction with impeller speed at 150 rpm at two different locations. The figure shows that the tangential velocity is higher near the impeller (line "60") than near the tank wall (line "30").

Solution concentration has also an important effect on the Reynolds number of the flow. Its effect combined with the impeller speed effect on Reynolds number is presented in **Figure 6.5.3** and **Table 6.5.1**.

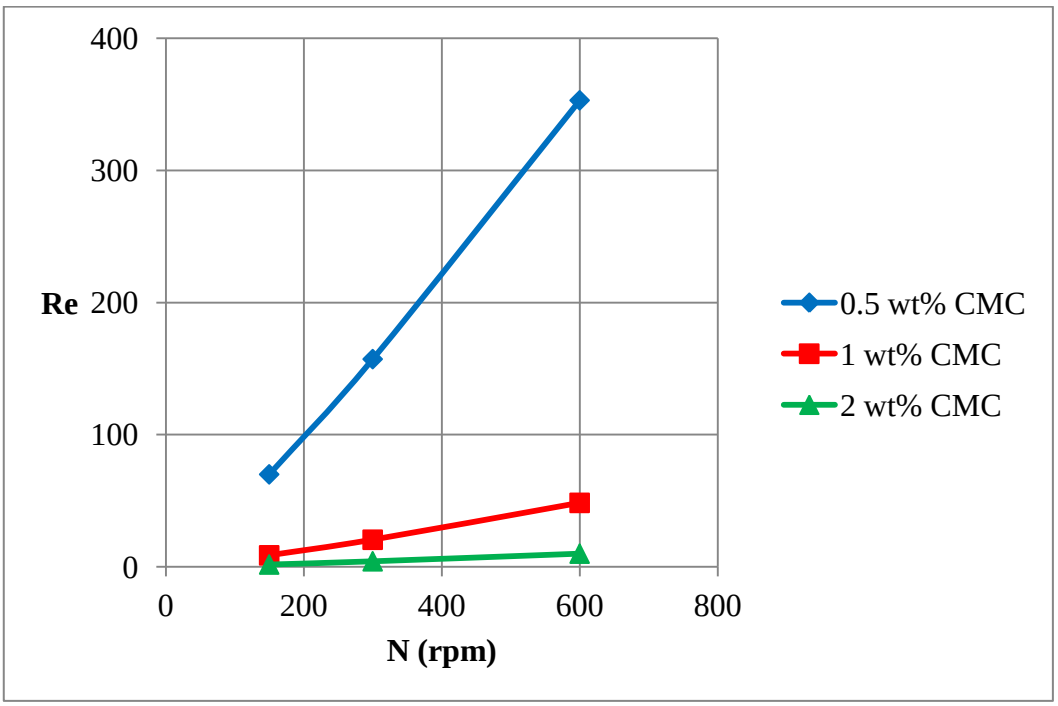

Figure 6.5.3 Effect of CMC Solution Concentration and Impeller Speed on Reynolds Number

Table 6.5.1 Effect of CMC Solution Concentration and Impeller Speed on Reynolds Number

CONCENTRATION	IMPELLER SPEED (rpm)	Re
0.5 wt% CMC	150	70
0.5 wt% CMC	300	157
0.5 wt% CMC	600	353
1 wt% CMC	150	9
1 wt% CMC	300	21
1 wt% CMC	600	48
2 wt% CMC	150	2
2 wt% CMC	300	4
2 wt% CMC	600	10

It can be observed that Reynolds number is increasing with increasing impeller speed and decreasing solution concentration. The relations are almost linear. In most of the cases, the flow is laminar. However, for 0.5 wt% CMC solution the flow regime corresponds to transition region at impeller speeds 300 rpm and 600 rpm.

6.6. Effect of Concentration and Impeller Speed on Mixing Time

Figure 6.6.1 shows the typical mixing time versus concentration plot for 0.5 wt% CMC solution agitated with 600 rpm. 95% of the concentration (which is accepted as complete mixing) is reached in 250 seconds. The mixing time measurement figures at the other impeller speeds and CMC concentrations are given in **APPENDIX C**.

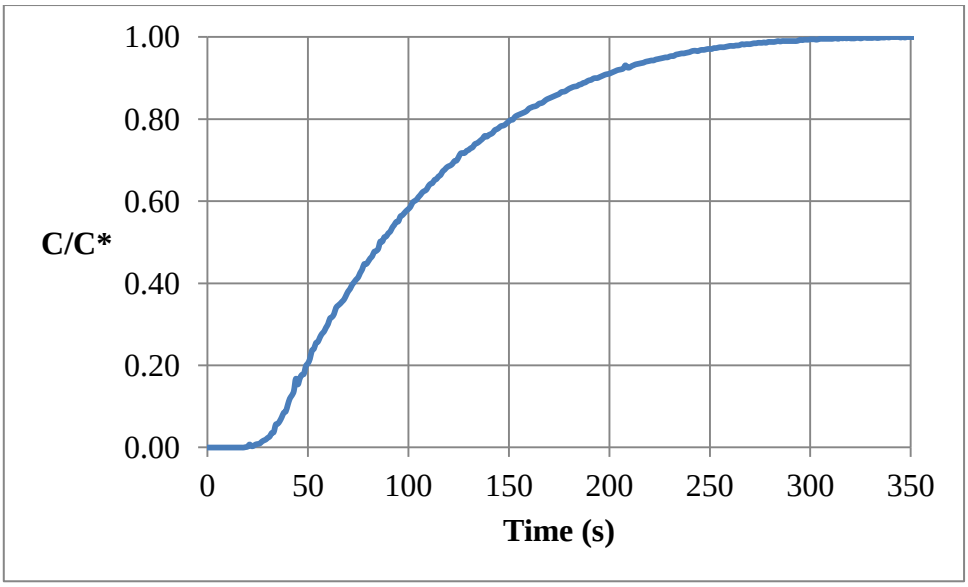

Figure 6.6.1 Mixing Time for 0.5 wt% CMC Solution at 600 rpm

The mixing time values for different CMC concentrations and impeller speeds are listed in **Table 6.6.1** and showed in **Figure 6.6.2**.

Table 6.6.1 Mixing Time Values

CONCENTRATION	IMPELLER SPEED	MIXING TIME
0.5 wt %	600 rpm	250 s
0.5 wt %	300 rpm	485 s
0.5 wt %	150 rpm	1300 s
1 wt %	600 rpm	230 s
1 wt %	300 rpm	820 s
1 wt %	150 rpm	2600 s

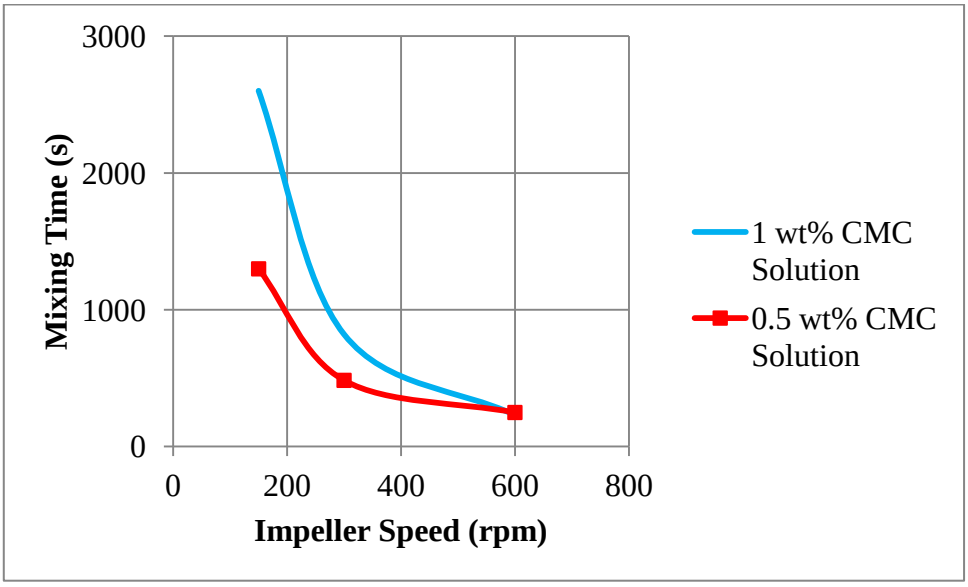

Figure 6.6.2 Mixing Time for 0.5 wt and 1 wt% CMC Solutions

Figure 6.6.2 shows the comparison of mixing time versus impeller speed plots for CMC solutions. 95% of the concentration (which is accepted as complete mixing) is reached in 2600 seconds for 1 wt% solution at 150 rpm. In this figure, it is observed that mixing time for 1 wt% CMC solutions are higher than mixing time for 0.5 wt % CMC solutions as expected. However, when the impeller speed is around 600 rpm, the mixing time different concentrations get closer to each other.

CHAPTER 7

CONCLUSIONS

To contribute to past and current studies on mixing, the hydrodynamics of carboxymethyl cellulose solution, which is predicted to be non-Newtonian, is studied in an agitated tank via Ultrasound Doppler Velocimeter and conductance measurements. Based on the results of this study, it is possible to draw the following conditions.

Some preliminary studies have been done in order to characterize rheological properties of CMC solutions used in this study. Analyzing the viscosity results, two important results have been identified: CMC solutions have shear-thinning property with very high viscosities, so CMC solutions are non-Newtonian type. Furthermore, salt addition to CMC solutions decreases the solution viscosity slightly up to 0.1 M concentration. The viscosity changes significantly with increasing salt concentration.

To characterize the velocity profile in the agitated tank, many measurements have been performed at several locations on the surface of the outer tank via UDV. The effect of solution concentration (viscosity of solution, in some other saying), impeller speed and probe location have been investigated. Concentrations studied are 0.5 wt%, 1 wt% and 2 wt%. Impeller speed changed between 150 rpm, 300 rpm and 600 rpm.

The results of UDV data analysis show that the measured tip velocity of the impeller decreases with increasing solution concentration. The velocity decreases near the walls of the tank and it reaches its maximum near the impeller tip as expected. In

other words, flow around the impeller is characterized by strong tangential and radial velocity components.

When the mixing time versus impeller speed plots for different concentrations of CMC solutions are investigated, it is seen that the mixing time increases with decreasing impeller speed and with increasing CMC solution concentration (i.e. viscosity). As expected, higher impeller speeds favors faster mixing in the solution. However, the dependence of mixing time on the impeller speed becomes weaker especially at high impeller speeds.

Considering the torque was the same, for all concentrations, power consumptions are 0.16 W for 150 rpm, 0.32 W for 300 rpm and 0.63 W for 600 rpm impeller speeds.

RECOMMENDATIONS

The aim of this study was to investigate experimentally the agitation hydrodynamics and estimate the mixing time of non-Newtonian solutions. To enhance this work, some recommendations can be done as below:

- The tank investigated in this study was a flat bottom tank. However, mostly round bottom tanks are used in the industry. Thus, the same procedure may be also applied for a round bottom tank also. The comparison of the results would be useful.
- There are auxiliary equipments in the market for 3D visualization of the flow by measuring with multiple probes connected to same UDV. Thus, they can be helpful to get a very fast and complete velocity profiling.
- During the mixing time experiments, NaCl (electrolytic tracer added to solution to observe the conductivity change) decreases the viscosity of CMC solution. Another electrolytic tracer which will not decrease the viscosity can be investigated.
- For torque measurements, a sensible torquemeter can be adapted.

REFERENCES

[1] Köseli, V., Zeybek, Ş., Uludağ, Y., 2006, *Online Viscosity Measurement of Complex Solutions Using Ultrasound Doppler Velocimetry*, Turk J Chem, 30:297-305

[2] Khopkar, A.R., Fradette, L., Tanguy, P.A., 2007, *Hydrodynamcis of a Dual Shaft Mixer with Newtonian and Non-Newtonian Fluids*, Trans IChemE, part A, Chemical Engineering Research and Design, 85(A6): 863-871

[3] Montante, G., Mostek, M., Jahoda, M., Magelli, F., 2005, *CFD Simulations and Experimental Validation of Homogenisation Curves and Mixing Time in stirred Newtonian and Pseudoplastic Liquids*, Chemical Engineering Science 60: 2427-2437

[4] Denn, M.M., 2004, *Fifty Years of non-Newtonian Fluid Dynamics*, AIChE Journal, October 2004, Vol. 50, No. 10, 2335-2345

[5] University of Delaware Mechanical Engineering Department, http://research.me.udel.edu/Last visited on July 2011

[6] Jaafar, W., et al., *Velocity and Turbulence Measurements by Ultrasound Pulse Doppler Velocimetry*, Measurement 42 (2009) 175-182

[7] Hui, L.K., et al., *Cavern Formation in Pulp Suspensions Using Side-entering Axial Flow Impellers*, Chemical Engineering Science 64 (2009) 509-519

[8] Pfund, D.M., et al., *Inline Ultrasonic Rheometry by Pulsed Doppler*, Ultrasonics 44 (2006) e477-482

[9] Dogan, N., et al., *Measurement of Polymer Melt Rheology using Ultrasonics-Based in-line Rheometry*, Meas. Sci. Technol. 16 (2005) 1684-1690

[10] Takeda, Y., *Measurement of velocity profile of mercury flow by ultrasound Doppler shift method,* Nucl. Techn. 79: 120-124 (1987)

[11] Sven ECKERT_, Dominique BUCHENAU, Gunter GERBETH, Frank STEFANI and Frank-Peter WEISS, *Some Recent Developments in the Field of Measuring Techniques and Instrumentation for Liquid Metal Flows*, Journal of NUCLEAR SCIENCE and TECHNOLOGY, Vol. 48, No. 4, p. 490–498 (2011)

[12] Y. Yeh and H.Z. Cummins, Localized fluid flow measurements with a He-Ne laser spectrometer, *Applied Physics Letters*, 4:176, 1964

[13] Albert D. Harvey 111 and Cassian K. Lee, Stuart E. Rogers, *Steady-State Modeling Measurement of a Baffled and Experimental Impeller Stirred Tank*, AXChE Journal October 1995 Vol. 41, No. 10, 2177-2186

[14] Broniarz, L., et al., *Mixing Time in Ionic and Non-Ionic Polymer Solutions*, 13th European Conference on Mixing, London, 14-17 April 2009

[15] D. Chappe, S. M. Kresta, A. Wall and A. Afacan, *The Effect of Impeller and Tank Geometry on Power number for a Pitched Blade Turbine,* Trans IChemE, Vol 80, Part A, May 2002

[16] Broniarz, L., et al., *Determination of the flow and heat transfer characteristics in non-Newtonian media agitated using the electrochemical technique,* International Journal of Heat and Mass Transfer 51 (2008) 910–919

[17] Dapia, S., et al., *Rheological behaviour of carboxymethylcellulose manufactured from TCF-bleached Milox pulps,* Food Hydrocolloids 19 (2005) 313–320

[18] Yang, X.H., et al., Viscosity properties of sodium carboxymethylcellulose solutions, Cellulose, 2007

[19] Mansour Jahangiri, *Fluctuation Velocity for Non-Newtonian Liquids in Mixing Tank by Rushton Turbine in the Transition Region*, Iranian Polymer Journal 15 (4), 2006, 285-290

[20] Marko Zlokarnik, *Stirring: Theory and Practice*, Wiley-VCH, Federal Republic of Germany, 2001

[21] Hayward Gordon Co., http://www.haywardgordon.com, Last visited on July 2011

[22] Tilton, J.N., *Perry's Chemical Engineers' Handbook,* 8th edition, McGraw-Hill, USA, 2008

[23] Signal Processing Co., http://www.signal-processing.com, Last visited on July 2011

[24] Sigma-Aldrich Co., http://www.sigmaaldrich.com/, Last visited on February 2011

[25] Brookfield Engineering Co., http://www.brookfieldengineering.com, Last visited on February 2011

[26] D. Chappe, S. M. Kresta, A. Wall and A. Afacan, *The Effect of Impeller and Tank Geometry on Power number for a Pitched Blade Turbine*, Trans IChemE, Vol 80, Part A, May 2002

APPENDIX A

ULTRASOUND DOPPLER VELOCIMETER DATA

Table A.1 Maximum Depth and Velocity data for US probes

f_0 (MHz)	P_{max} (mm)	V_{max} (mm/s)	P_{max} V_{max} (mm^2/s)	ΔV (mm/s)
0.5	100	5476	547,600	43.1
	750	730.1	547,600	5.7
1	100	2738	273,800	21.6
	750	365.1	273,800	2.9
2	100	1369	136,900	10.8
	750	182.5	136,900	1.4
4	100	684.5	68,450	5.4
	750	91.3	68,450	0.7
8	100	342.3	34,225	2.7
	750	45.6	34,225	0.4

APPENDIX B

EFFECT OF POSITION ON VELOCITY PROFILE

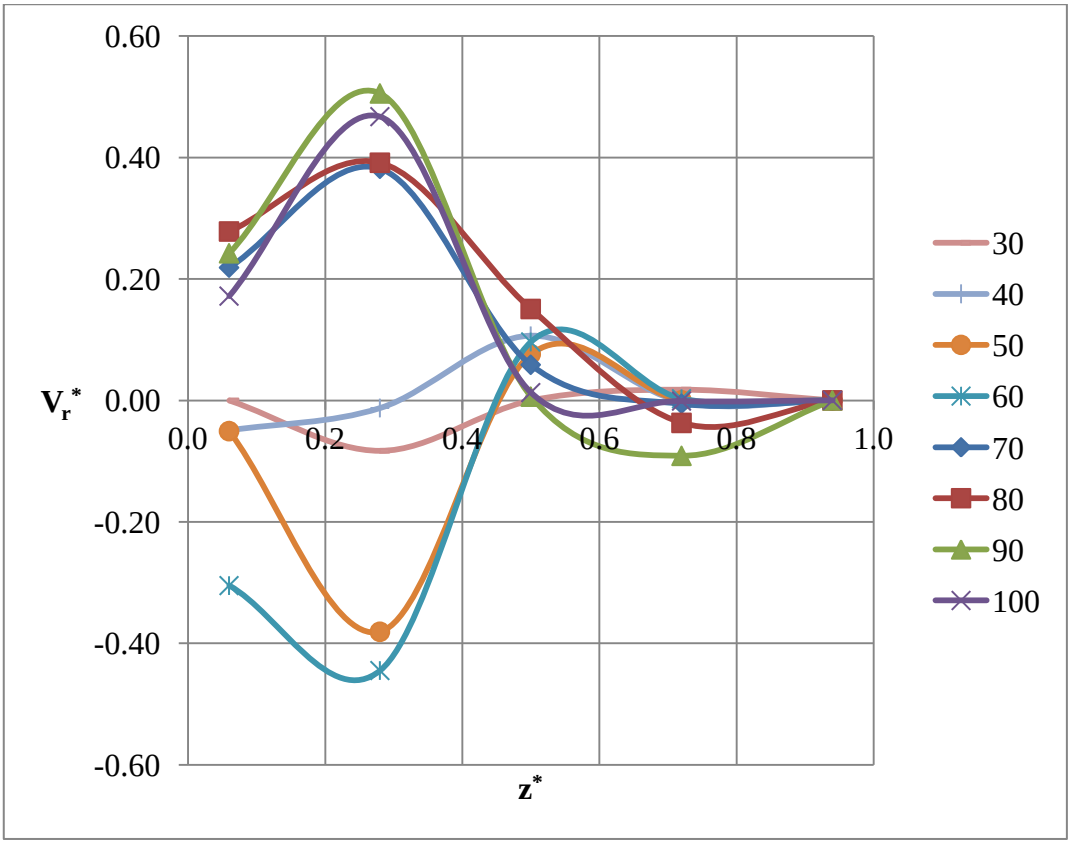

Figure B.1 Velocity Distribution at C Line for 1 wt% CMC Solution with 150 rpm

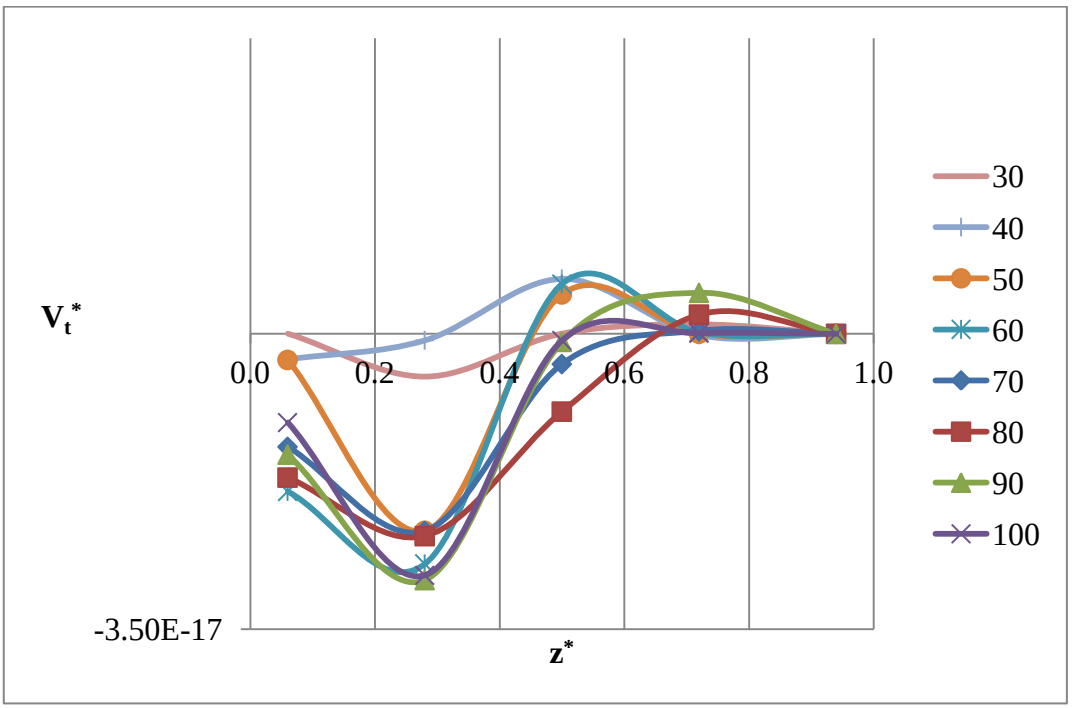

Figure B.2 Velocity Distribution at C Line for 1 wt% CMC Solution with 150 rpm

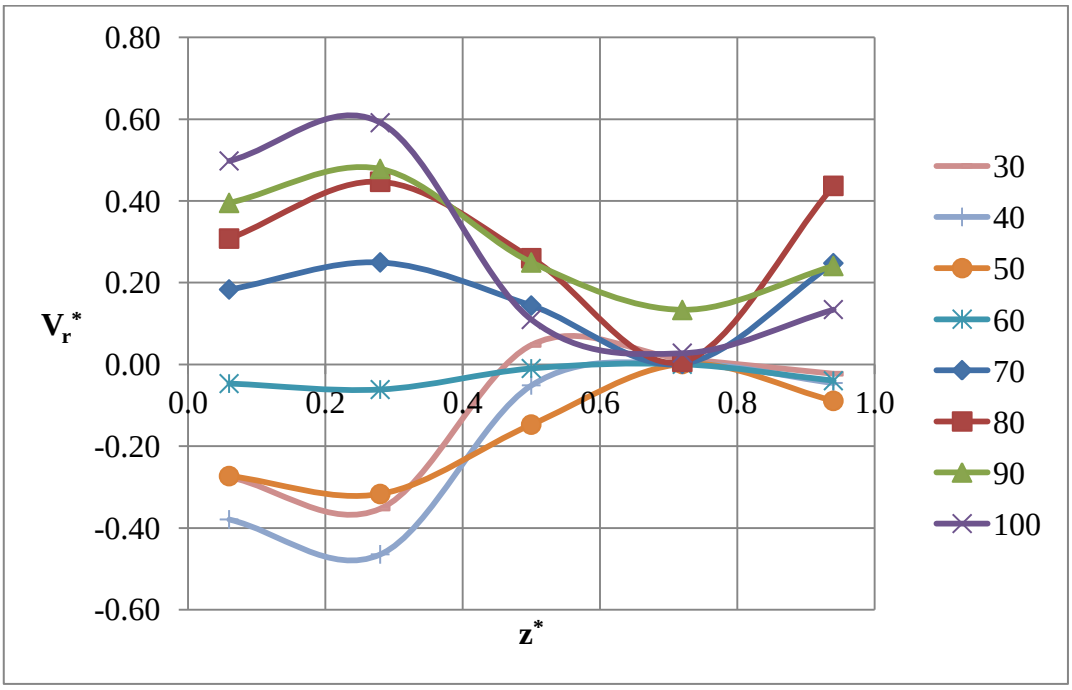

Figure B.3 Velocity Distribution at D Line for 1 wt% CMC Solution with 150 rpm

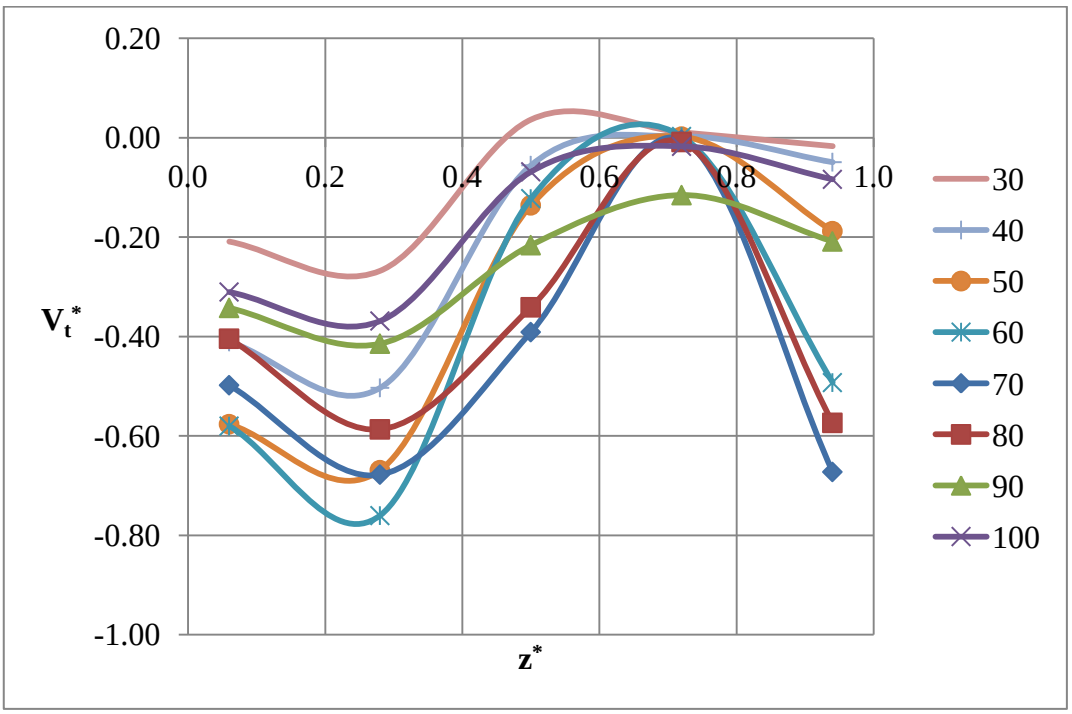

Figure B.4 Velocity Distribution at D Line for 1 wt% CMC Solution with 150 rpm

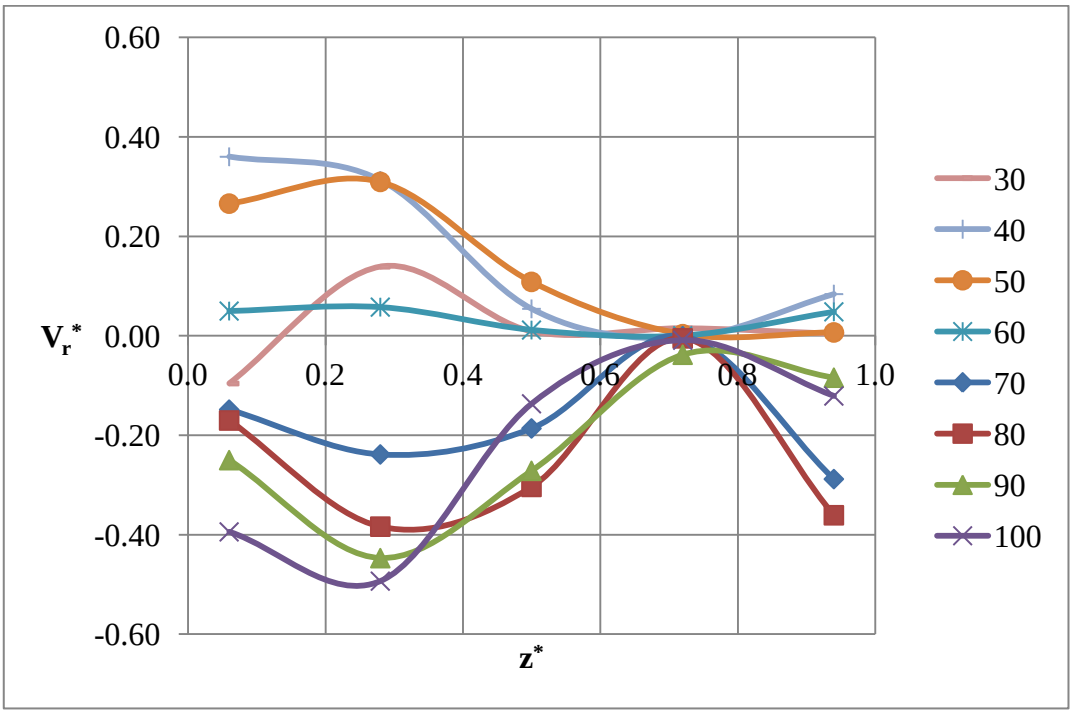

Figure B.5 Velocity Distribution at B Line for 1 wt% CMC Solution with 300 rpm

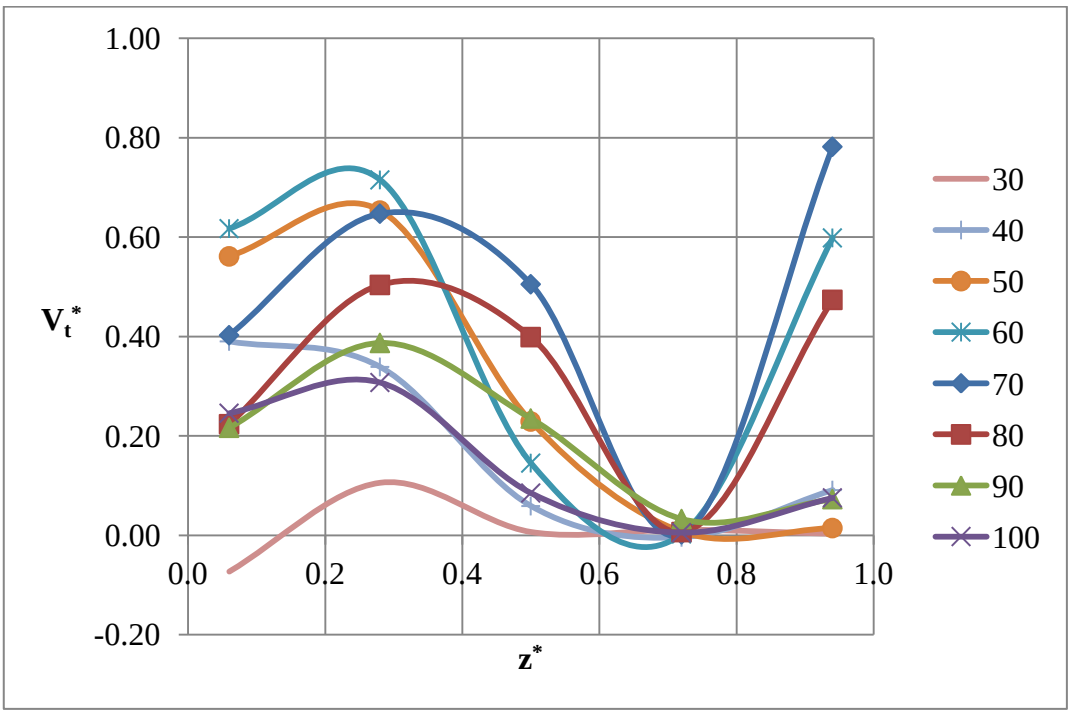

Figure B.6 Velocity Distribution at B Line for 1 wt% CMC Solution with 300 rpm

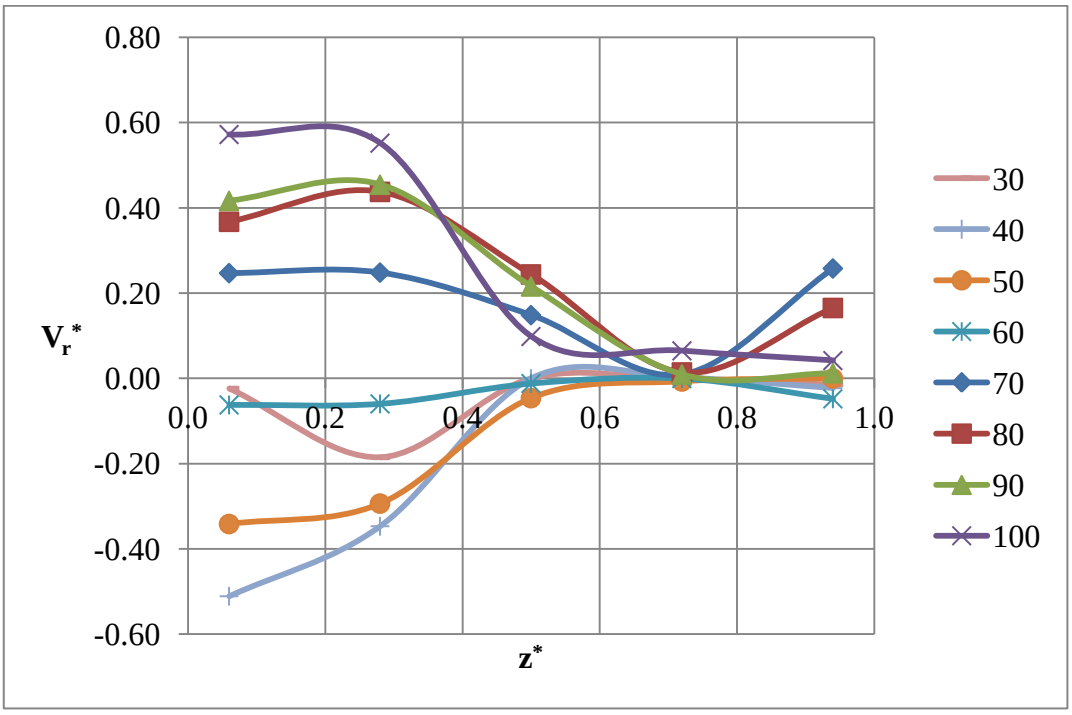

Figure B.7 Velocity Distribution at D Line for 1 wt% CMC Solution with 300 rpm

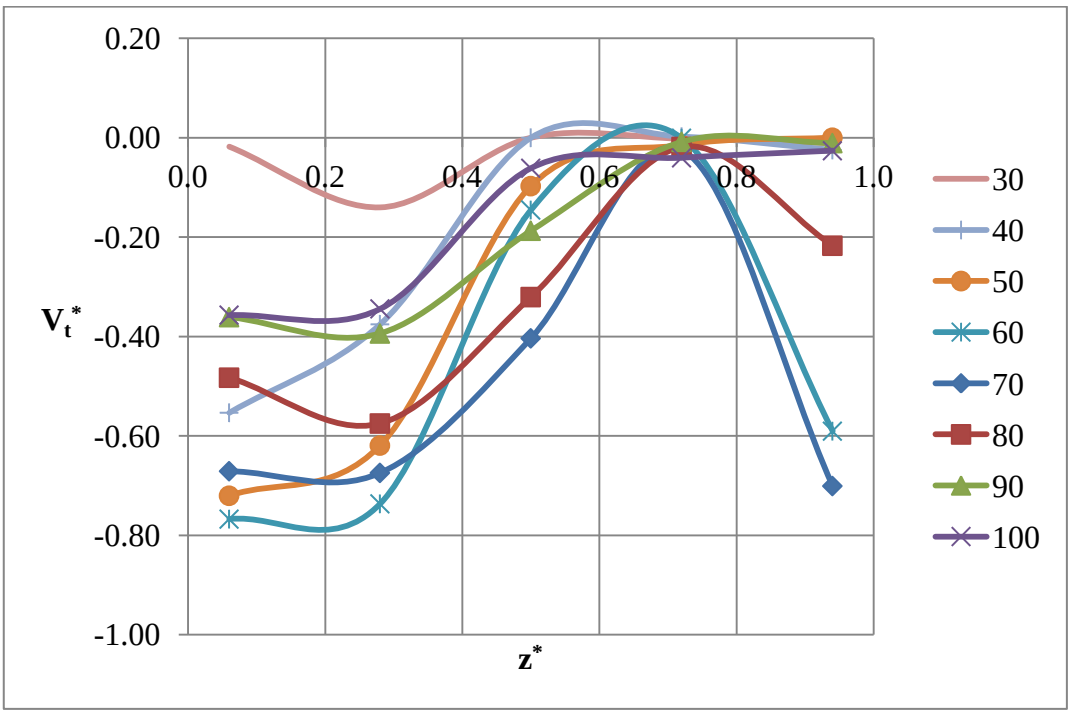

Figure B.8 Velocity Distribution at D Line for 1 wt% CMC Solution with 300 rpm

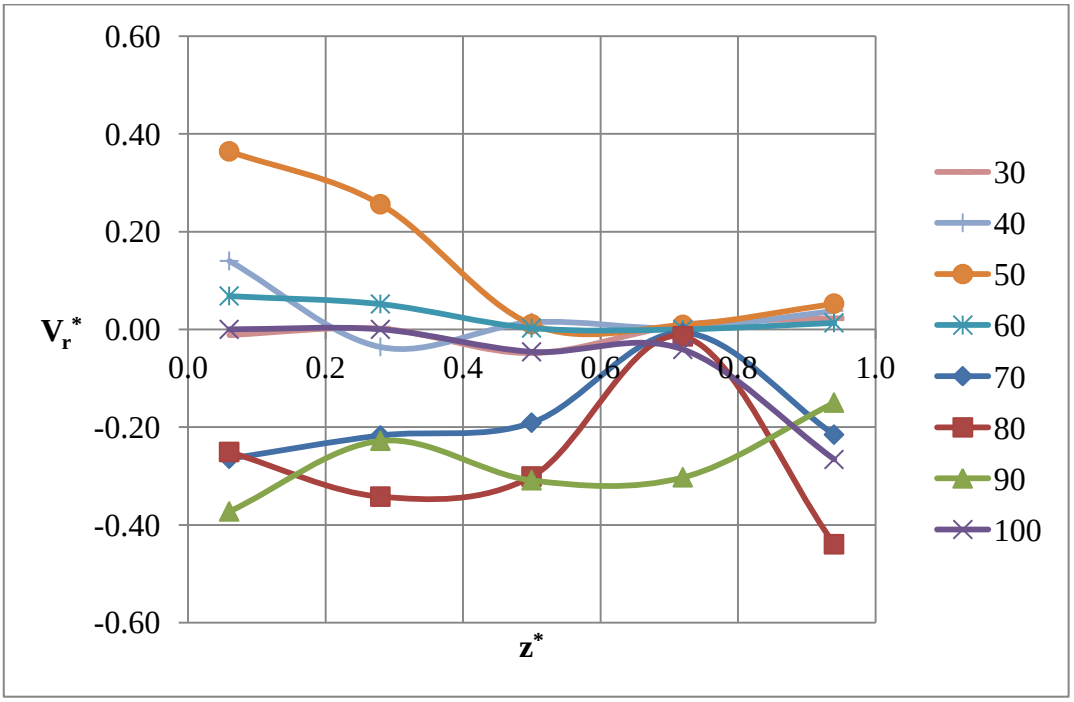

Figure B.9 Velocity Distribution at B Line for 1 wt% CMC Solution with 600 rpm

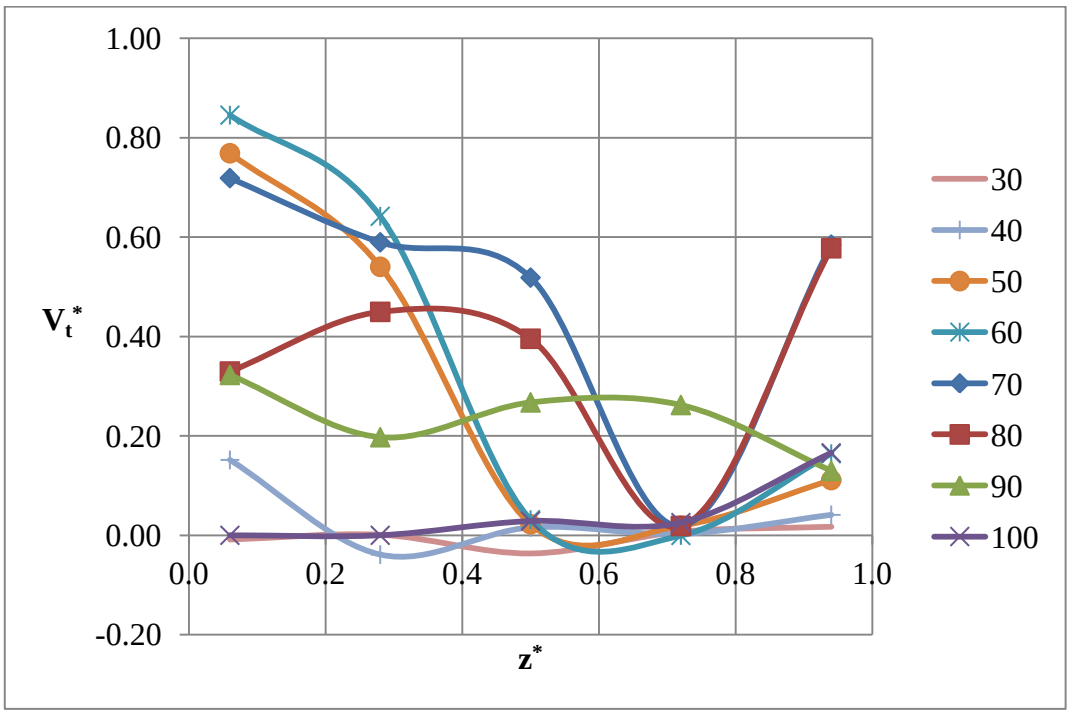

Figure B.10 Velocity Distribution at B Line for 1 wt% CMC Solution with 600 rpm

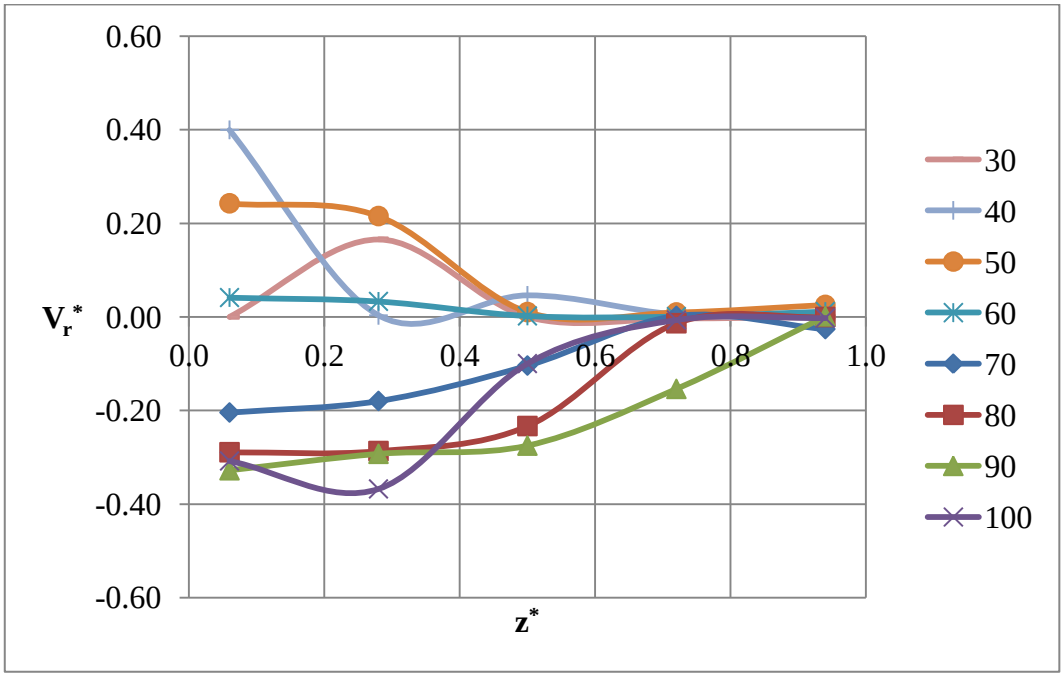

Figure B.11 Velocity Distribution at B Line for 0.5 wt% CMC Solution with 150 rpm

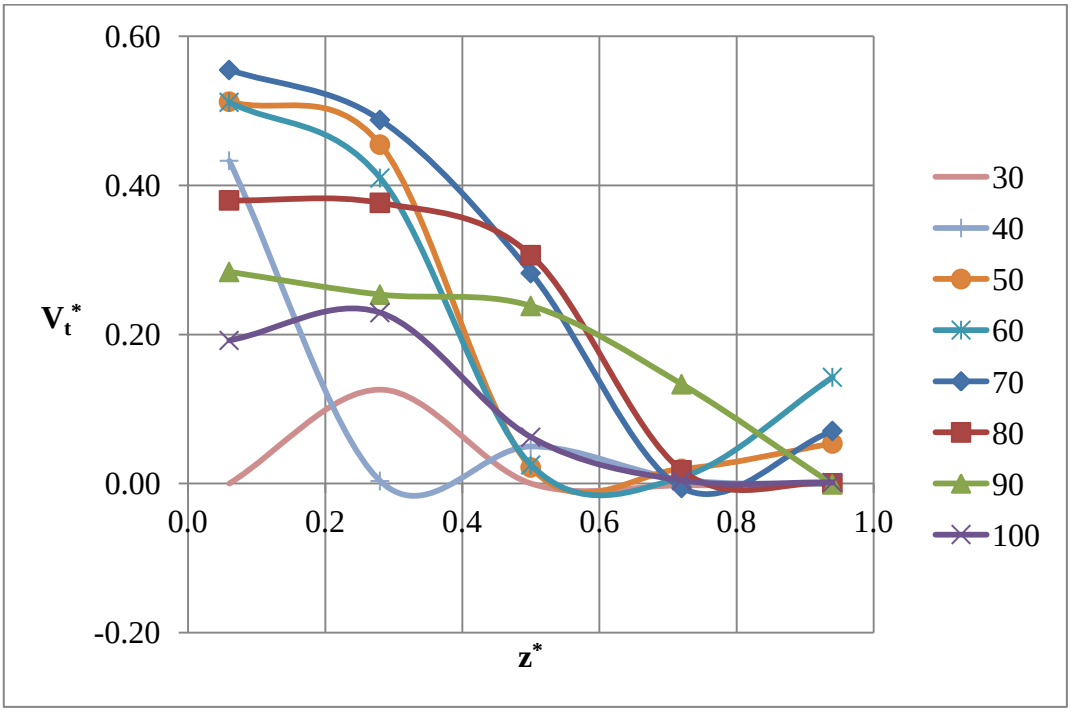

Figure B.12 Velocity Distribution at B Line for 0.5 wt% CMC Solution with 150 rpm

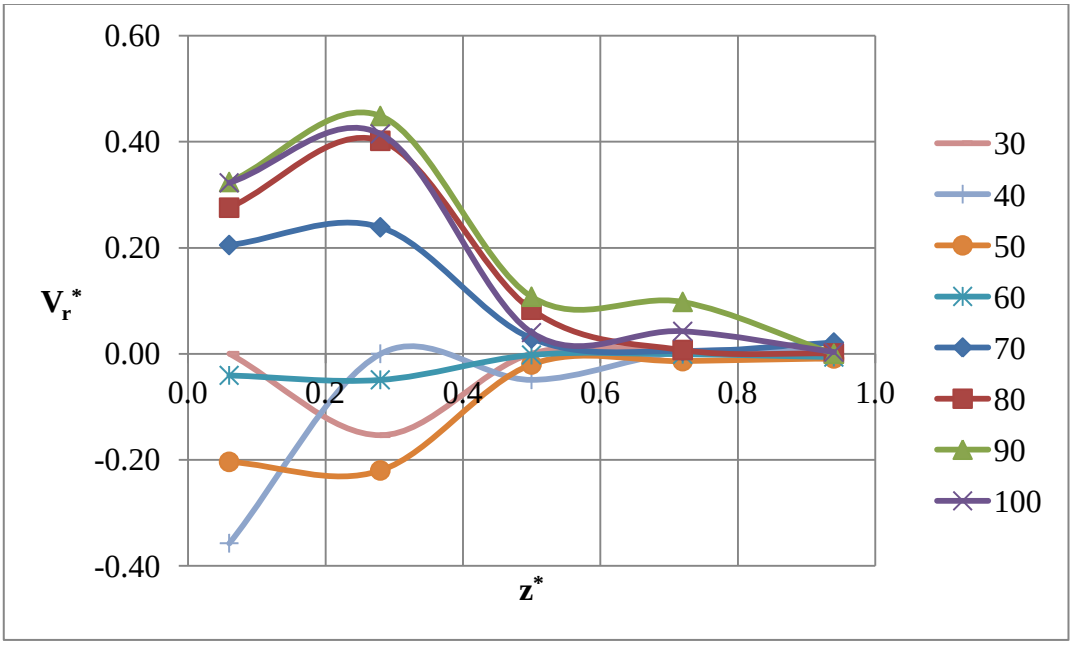

Figure B.14 Velocity Distribution at D Line for 0.5 wt% CMC Solution with 150 rpm

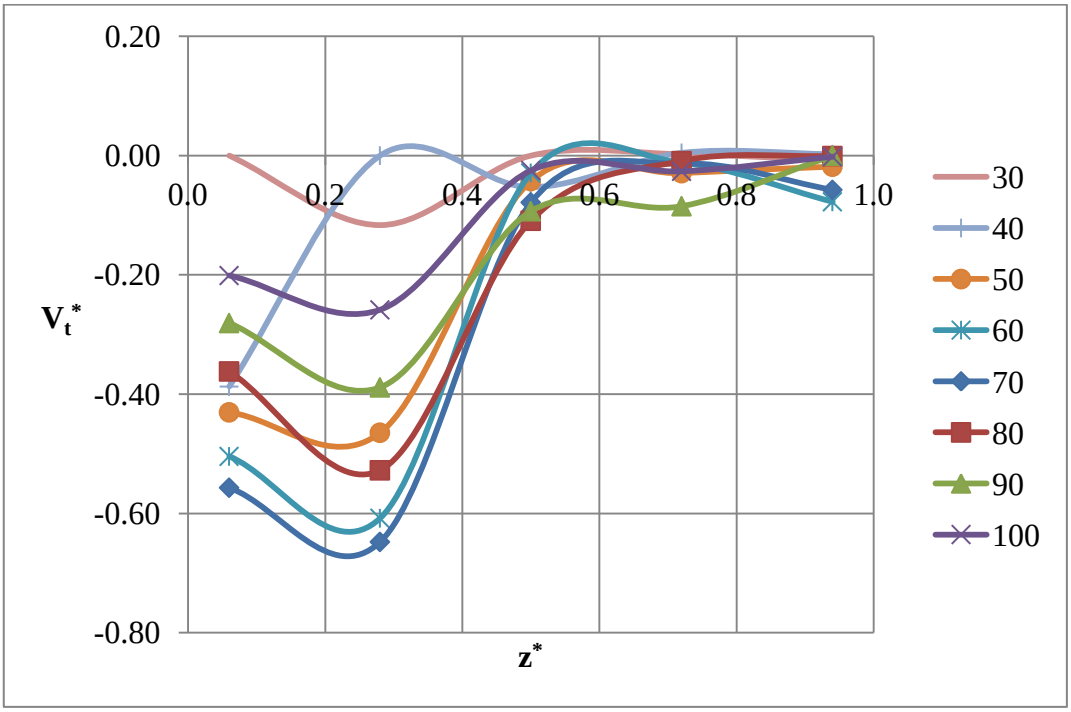

Figure B.15 Velocity Distribution at D Line for 0.5 wt% CMC Solution with 150 rpm

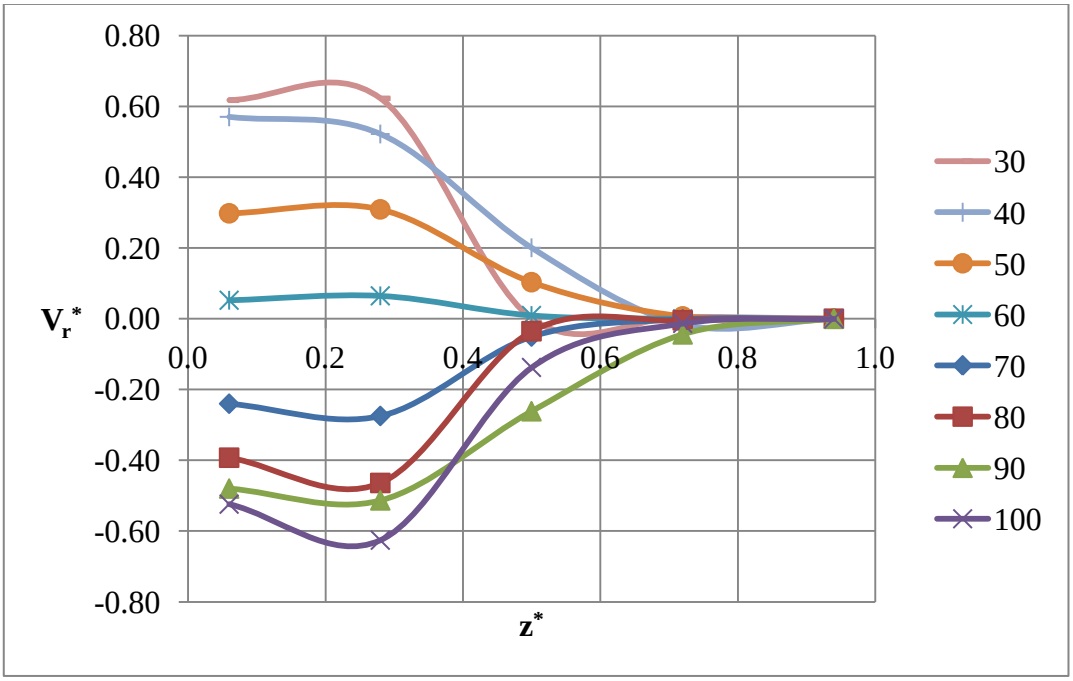

Figure B.16 Velocity Distribution at B Line for 0.5 wt% CMC Solution with 300 rpm

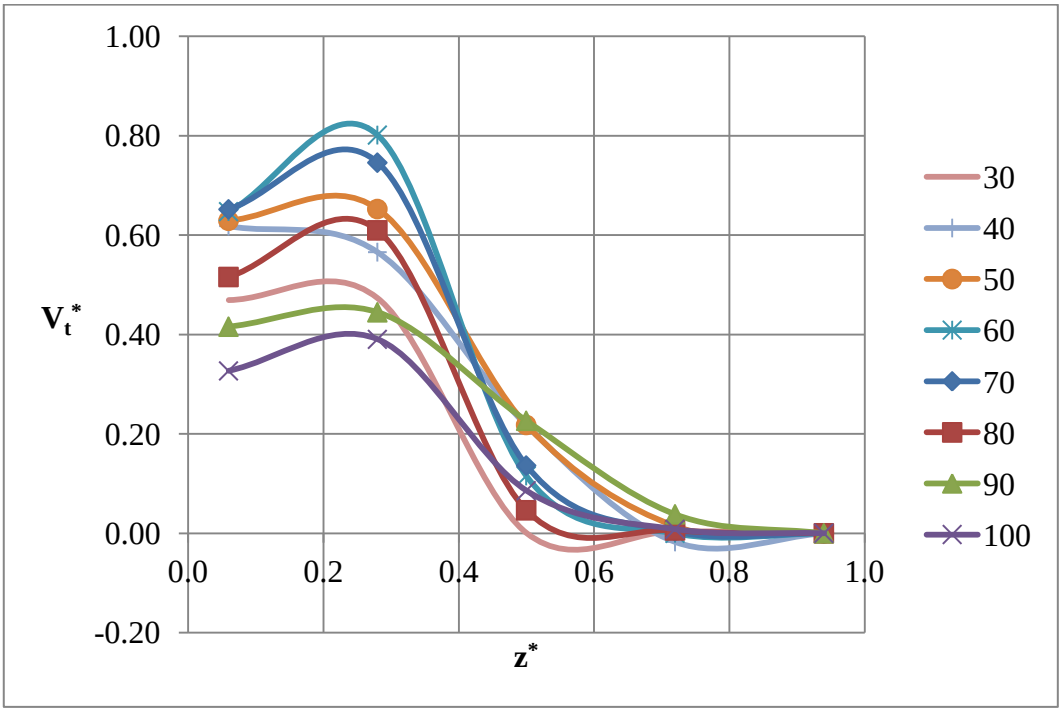

Figure B.17 Velocity Distribution at B Line for 0.5 wt% CMC Solution with 300 rpm

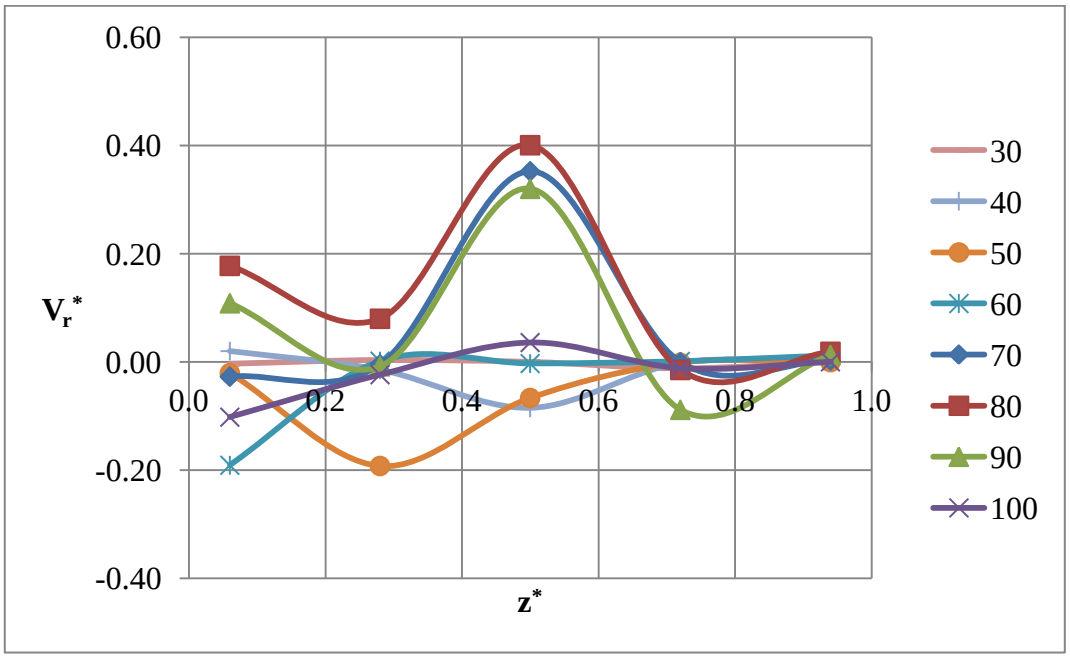

Figure B.18 Velocity Distribution at C Line for 0.5 wt% CMC Solution with 300 rpm

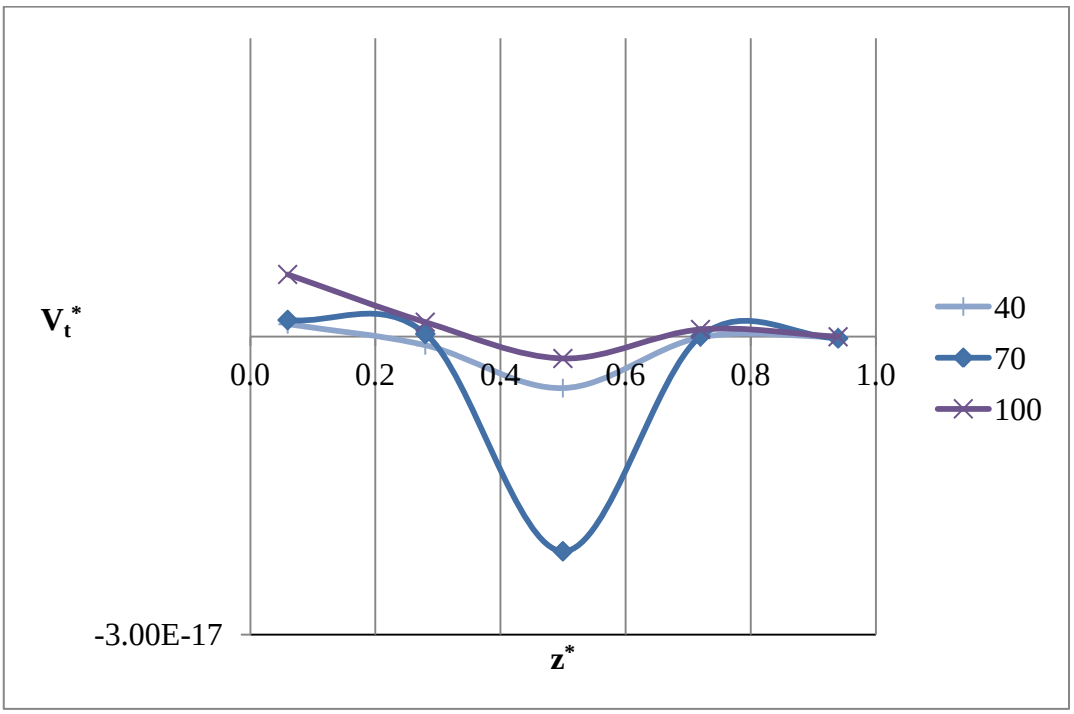

Figure B.19 Velocity Distribution at C Line for 0.5 wt% CMC Solution with 300 rpm

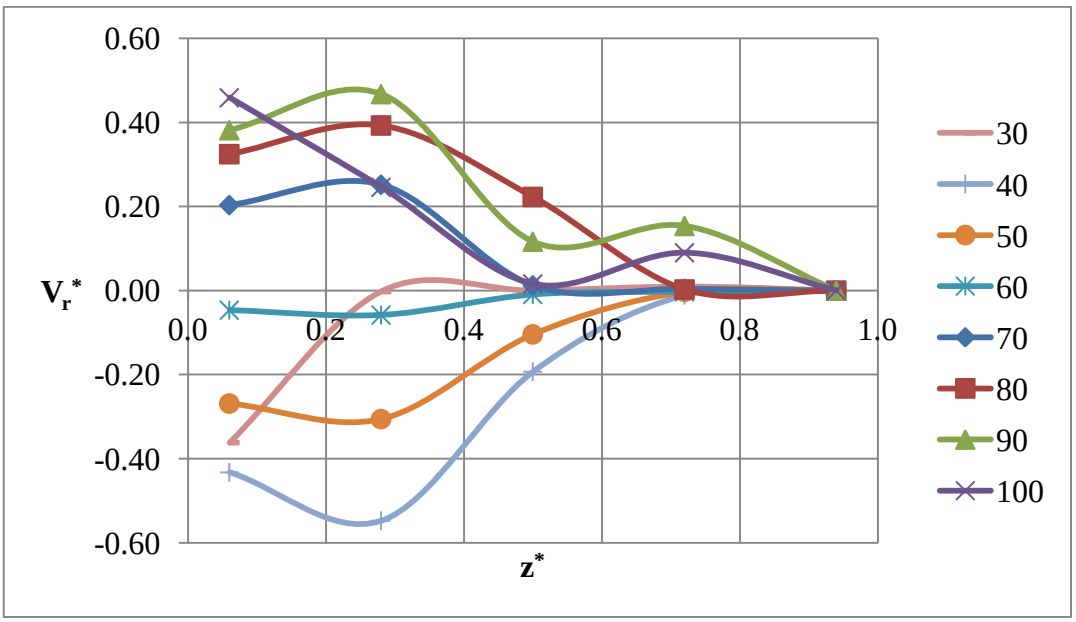

Figure B.20 Velocity Distribution at D Line for 0.5 wt% CMC Solution with 300 rpm

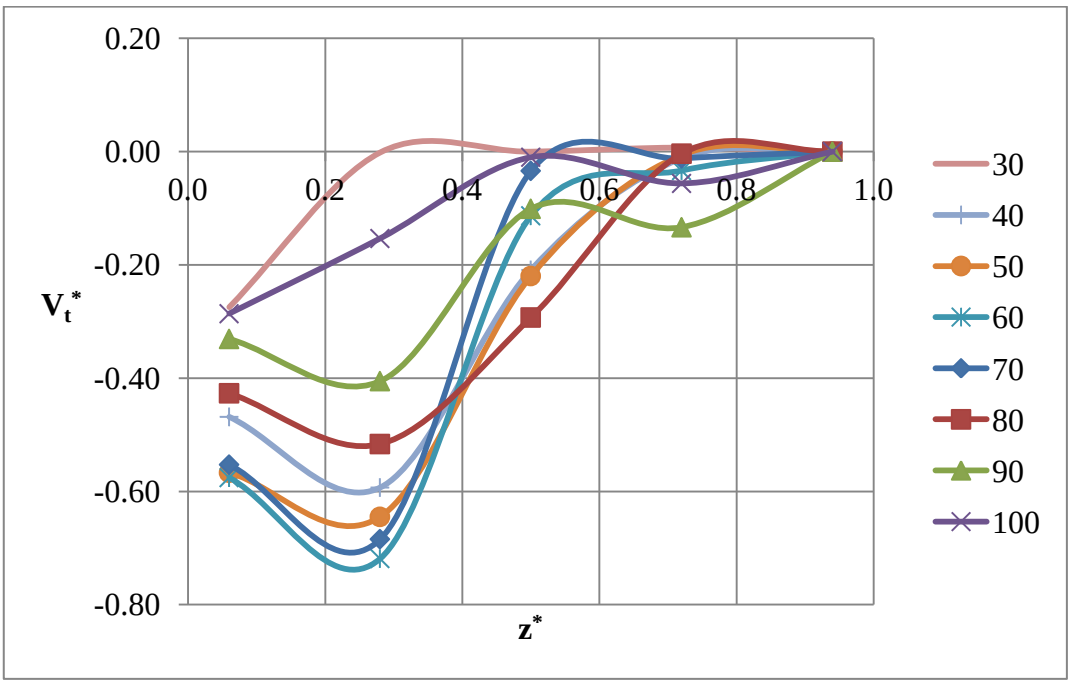

Figure B.21 Velocity Distribution at D Line for 0.5 wt% CMC Solution with 300 rpm

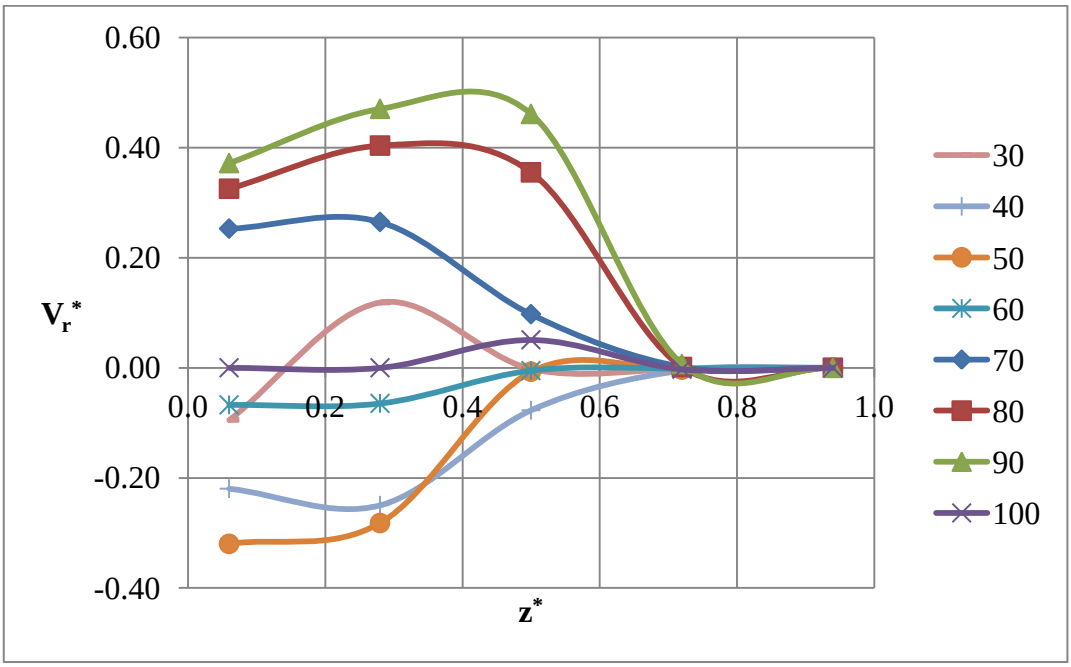

Figure B.22 Velocity Distribution at D Line for 0.5 wt% CMC Solution with 600 rpm

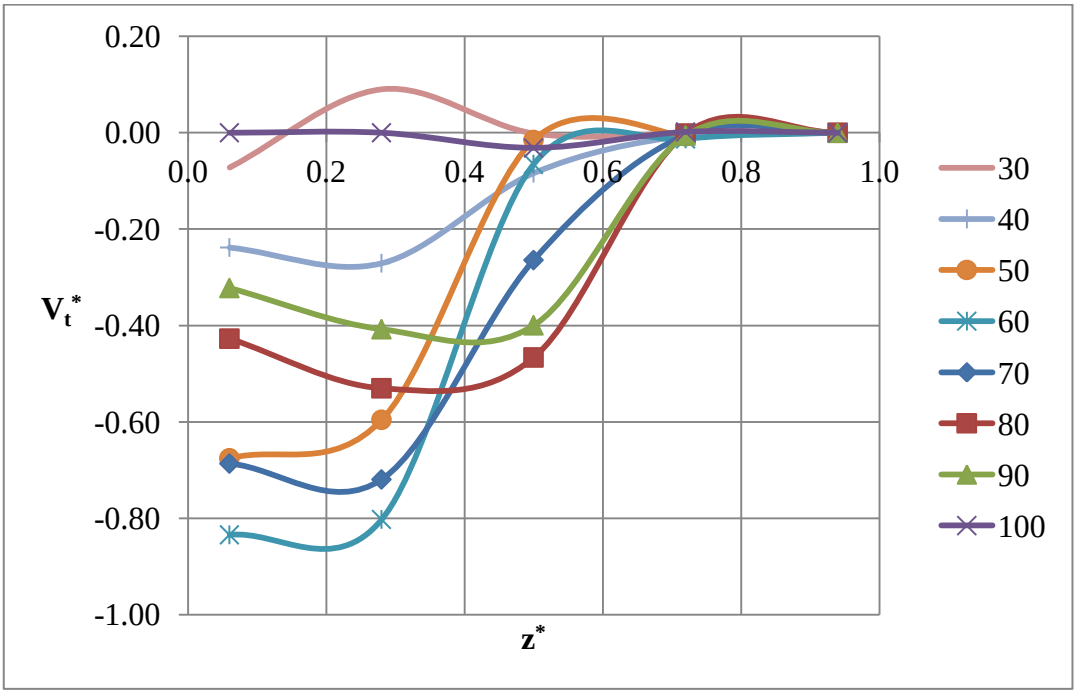

Figure B.23 Velocity Distribution at D Line for 0.5 wt% CMC Solution with 600 rpm

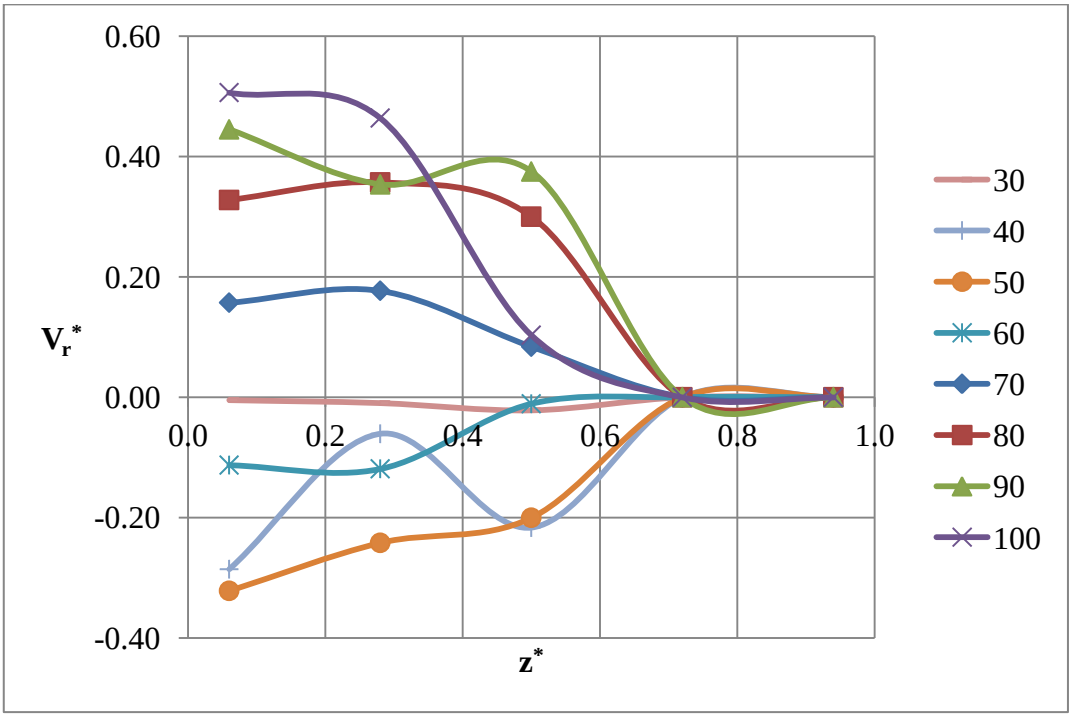

Figure B.24 Velocity Distribution at D Line for 2 wt% CMC Solution with 300 rpm

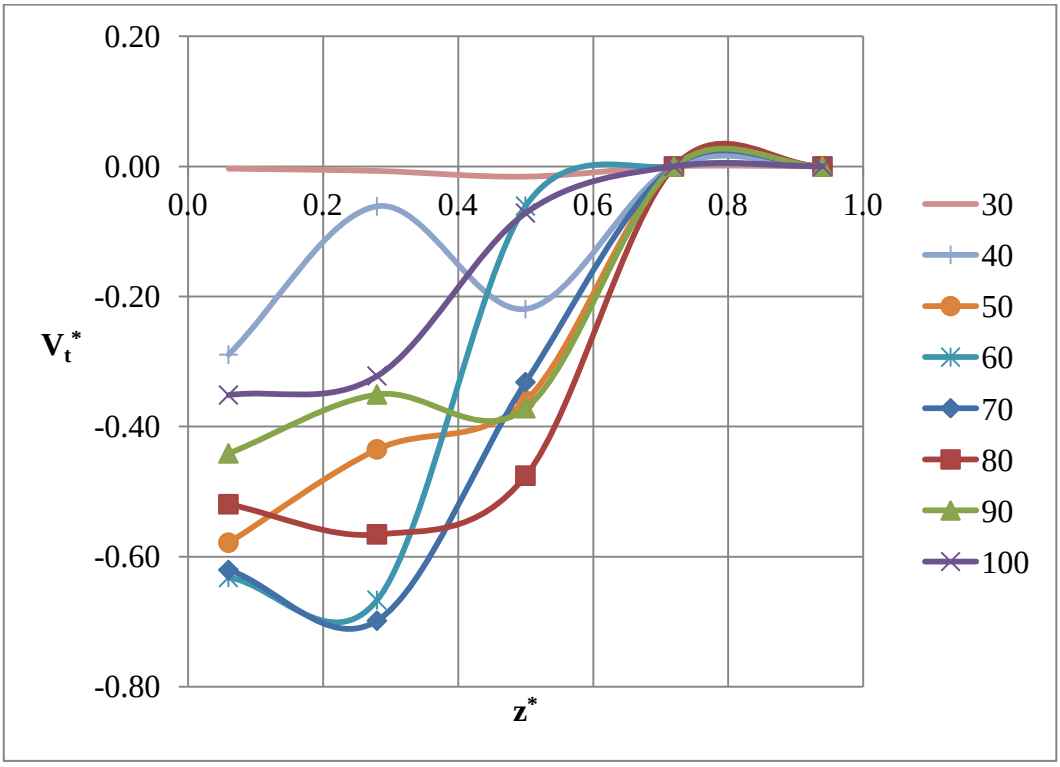

Figure B.25 Velocity Distribution at D Line for 2 wt% CMC Solution with 300 rpm

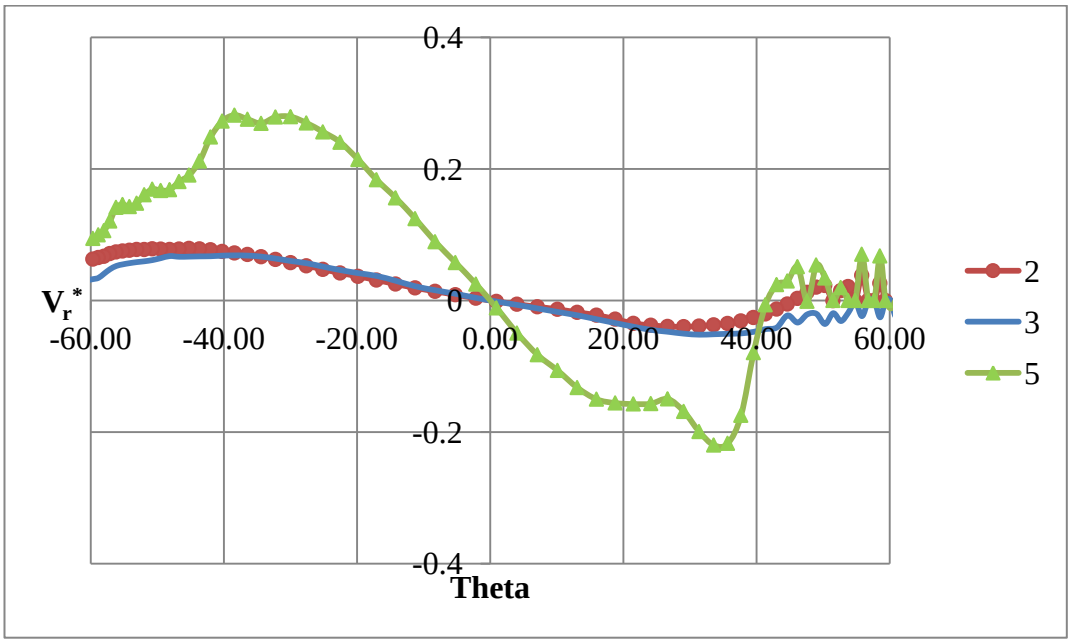

Figure B.26 Velocity Distribution at D Line for 2 wt% CMC Solution with 600 rpm

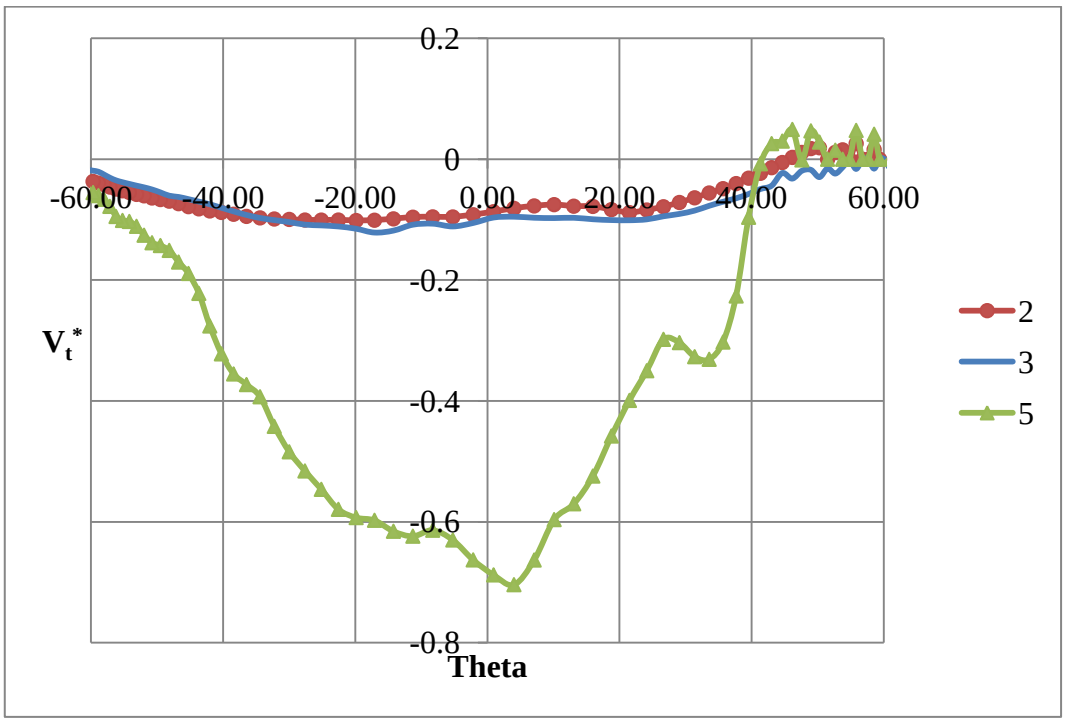

Figure B.27 Velocity Distribution at D Line for 2 wt% CMC Solution with 600 rpm

Figure B.26 and **Figure B.27** show the radial and the tangential velocity distributions in the 2 wt% CMC solution along the z-axis at D line direction with impeller speed at 600 rpm with respect to angular position. Line "2" and Line "3" are near the top of the tank. Line "5" is at the bottom of the tank. These plots are just to show how the raw data looks like. However, even with this raw data, it can be concluded that velocity is higher near the impeller region than upper parts of the tank. The tangential component of the measured velocity near the impeller is 70% of the theoretical value of impeller tip velocity.

APPENDIX C

EFFECT OF IMPELLER SPEED AND CONCENTRATION ON MIXING TIME

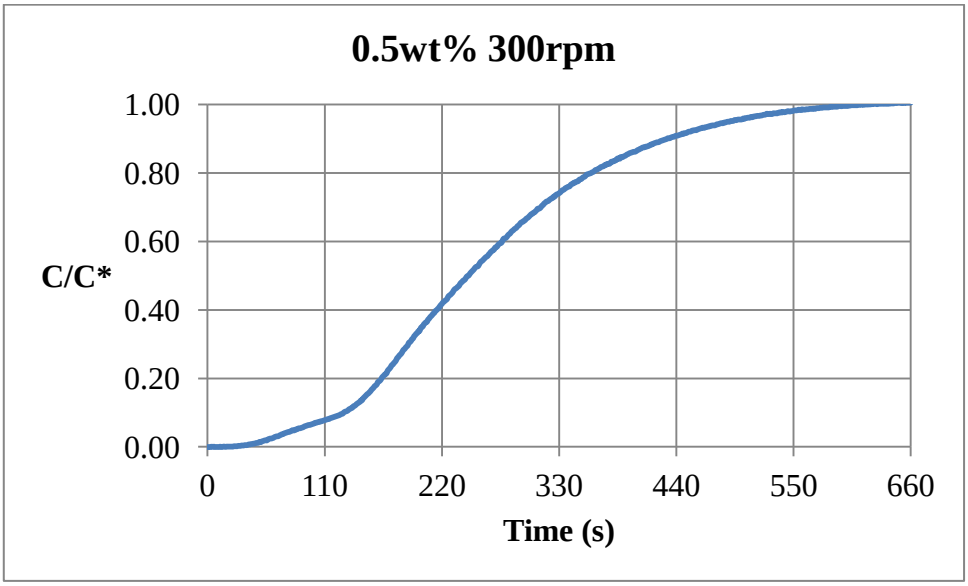

Figure C.1 Mixing Time for 0.5 wt% CMC Solution at 300 rpm

Figure C.1 shows the mixing time versus concentration plot for 0.5 wt% CMC solution agitated with 300 rpm. 95% of the concentration (which is accepted as complete mixing) is reached in 485 seconds.

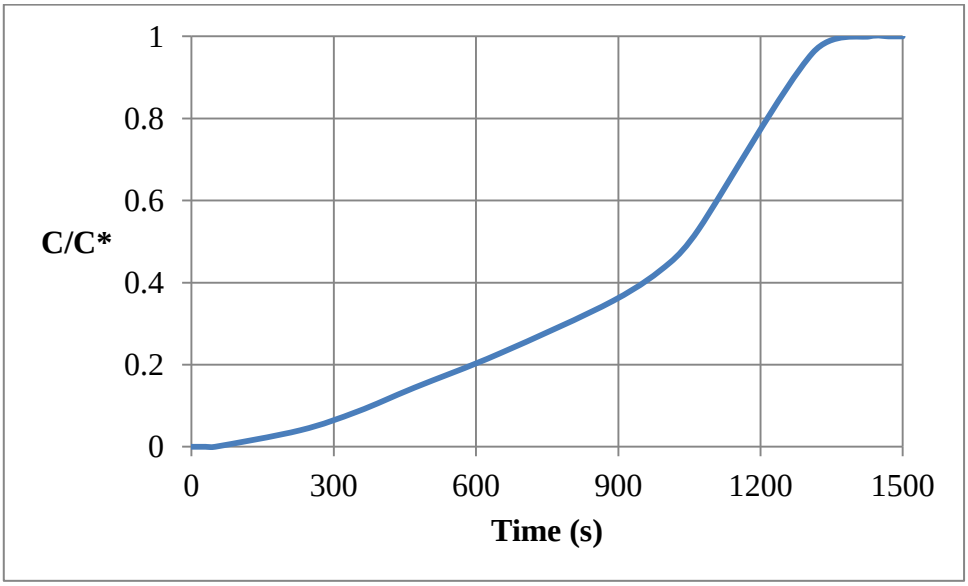

Figure C.2 Mixing Time for 0.5 wt% CMC Solution at 150 rpm

Figure C.2 shows the mixing time versus concentration plot for 0.5 wt% CMC solution agitated with 150 rpm. 95% of the concentration (which is accepted as complete mixing) is reached in 1300 seconds.

Figure C.3 shows the mixing time versus concentration plot for 1 wt% CMC solution agitated with 600 rpm. 95% of the concentration (which is accepted as complete mixing) is reached in 230 seconds.

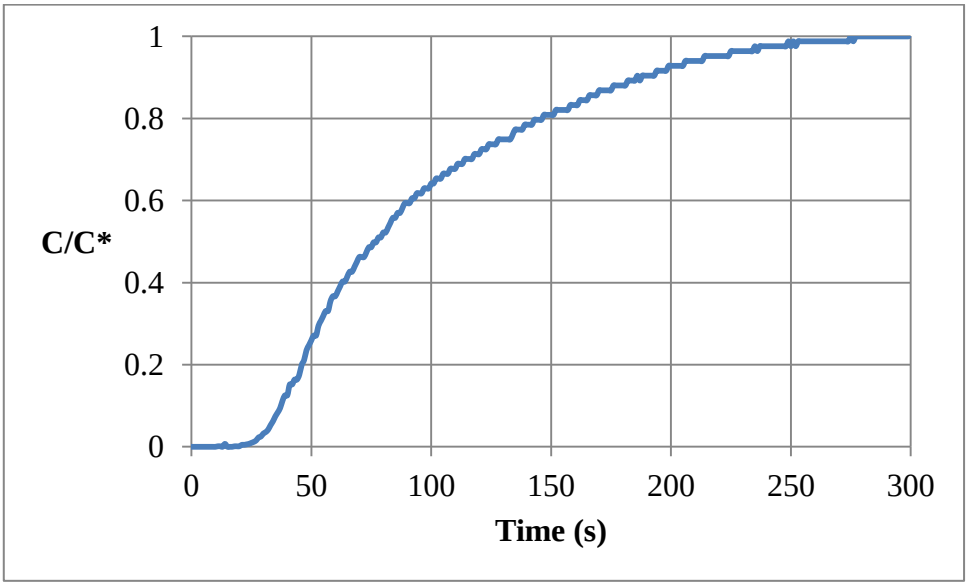

Figure C.3 Mixing Time for 1 wt% CMC Solution at 600 rpm

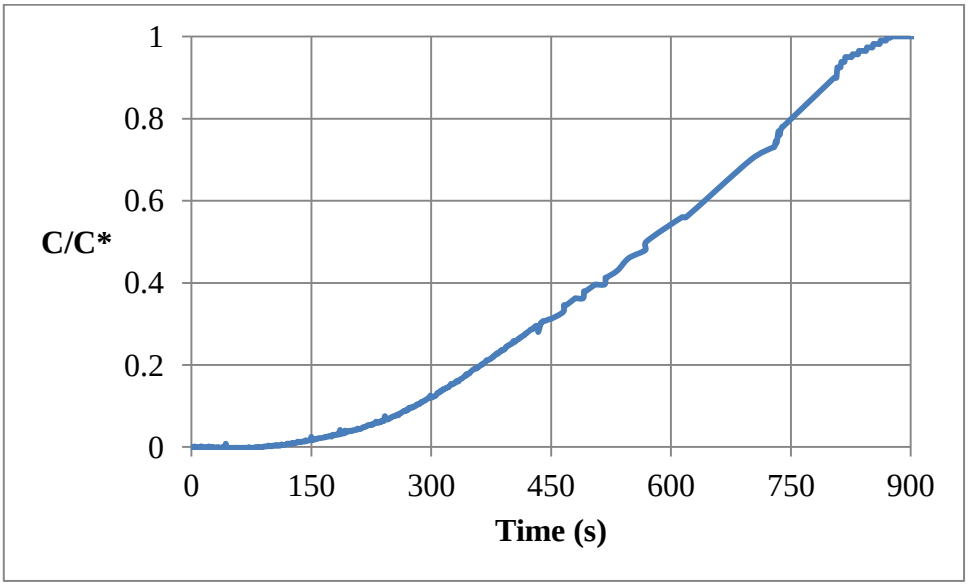

Figure C.4 Mixing Time for 1 wt% CMC Solution at 300 rpm

Figure C.4 shows the mixing time versus concentration plot for 1 wt% CMC solution agitated with 300 rpm. 95% of the concentration (which is accepted as complete mixing) is reached in 820 seconds.

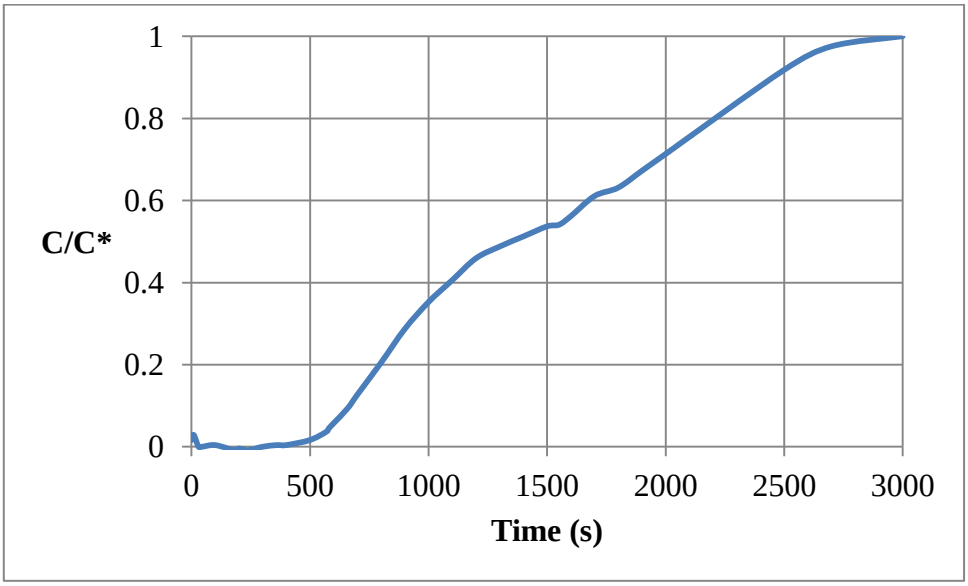

Figure C.5 Mixing Time for 1 wt% CMC Solution at 150 rpm

Figure C.5 shows the mixing time versus concentration plot for 1 wt% CMC solution agitated with 150 rpm. 95% of the concentration (which is accepted as complete mixing) is reached in 2600 seconds.